Nanotopographical modifications of biomedical implants

By

Shahram Riahinezhad

Master of Science in Engineering Physics-Mechanical Engineering

University of Central Oklahoma

Edmond, Oklahoma

2016

Master Thesis

Submitted to the Faculty of

the Graduate collage of the University of Central Oklahoma

in partial fulfillment of the requirements for Degree of

Master of Science

June, 2016

Nanotopographical modifications of biomedical implants

Thesis Approved:

Committee Chair: Dr. Morshed Khandaker

Committee Member: Dr. Mohammad Hossan

Committee Member: Dr. Abdellah Ait Moussa

ACKNOWLEDGMENTS

I would like to express my deepest sense of appreciation to my advisor, Dr. Morshed khandaker, for the continuous support of my master study and research, for his patience, motivation, enthusiasm, and immense knowledge. His guidance helped me in all the time of research and writing of this thesis. I could not have imagined having a better advisor and mentor for my master study.

I am thankful to Dr. Mohammad Hossan and Dr. Abdellah Ait Moussa for their encouragement, insightful comment, and support during my research.

I acknowledge my gratitude to the National Institute of General Medical Sciences of the National Institutes of Health under award number, 5P20GM103447. I am also indebted to the Department of Engineering and Physics, the College of Mathematics and Science, and Graduate collage at University of Central Oklahoma.

I would like to thanks my professors during the graduate studies and my research mate Yanling Li, Charles Collins for cooperation and guidance.

Finally, I take this opportunity to express the profound gratitude from my deep heart to my beloved wife, children, and parents for their love and continuous support. I also would like to thank my uncle, Hooshang, for his support.

Nanotopographical modifications of biomedical implants

Abstract

Implant failure due to poor integration of the implant with the native tissue is a common problem in various orthopedic and orthodontic implants. Nanotopographical modifications of an implant surface such as; surface roughness, surface energy, and thin film coating can enhance the mechanical and biological functions of an implant. This study used three nanotopographical modifications techniques; peening, plasma, and electrospun nanofiber to improve the mechanical and biological functions of metallic and polymeric implants. Laser peening, plasma nitridation and electrospun nanofiber coating techniques were used to improve the mechanical and biological functions of titanium implant. Electrospun nanofiber coating techniques were used to design polyethylene Glycol Diacrylate (PEGDA) and silicone based tissue engineering scaffold for bone substitute and intervertebral disc, respectively. This study found significant improvement of titanium mechanical stability with cement due to the application of plasma and peen treatment on titanium surface. Also, this study delivered a novel collagen – poly (ε-caprolactone) (PCL) electrospun nanofiber biocoating technique (patent pending) for metal implant that can significantly improve the *in vivo* mechanical stability and osseointegration. Furthermore, a novel bone graft material (patent pending) was fabricated by sandwiching multi-layers of PEGDA and PCL electrospun fiber. Finally, a novel intervertebral disc implant (patent pending) was created by anchoring silicone gels using PCL electrospun fiber that mimics the architecture of human intervertebral disc.

TABLE OF CONTENTS

ACKNOWLEDGMENTS ii

LIST OF FIGURES xii

LIST OF TABLES xv

LIST OF ABBREVIATION xvi

1 INTRODUCTION 1

1.1 Electrospinning 1

1.2 Implant fixation technique 1

1.3 Implants investigated in this study 2

1.3.1 Titanium 2

1.3.2 Bone Cement 2

1.3.3 PEGDA 3

1.3.4 Silicone 4

1.4 Modification of implant surface 4

1.4.1 Peen treatment 4

1.4.2 Plasma treatment 4

1.4.3 Nanofiber and nanoparticles 4

1.5 Motivation and goals 5

1.6 Objectives 5

1.7 Organization of the thesis 5

1.8 Figures 7

2 PEEN TREATMENT ON TITANIUM IMPLANT 9

2.1 Background and specification 10

2.1.1 Introduction 10

2.1.2 Research questions 11

2.1.3 Scope of work 12

2.2 Material and method 12

2.2.1 Sample Preparation 12

2.2.2 Polishing protocol 13

2.2.3 Laser peening treatment on Ti 13

2.2.4 Surface roughness and morphology 13

2.2.5 Mechanical tests on Ti/cement samples 14

2.3 Result 15

2.4 Discussion 16

2.5 Conclusion 17

2.6 Figures 18

2.7 Tables 21

3 DIRECT CURRENT GLOW DISCHARGE NITROGEN PLASMA TREATMENT ON TITANIUM IMPLANT 22

3.1Summary 22

3.2Background and specification 22

3.2.1Introduction 22

3.3Material and method 24

3.3.1Sample Preparation 24

3.3.2Nitrogen-plasma treatment 25

3.3.3Surface morphology 26

3.3.5Pull out tension tests on titanium/cement samples 26

3.3.6Statistical Analysis 27

3.4Results 27

3.5 Discussion 28

3.6 Conclusion 30

3.8Tables 34

4 IN VIVO EVALUATION OF THE ELECTROSPIN FIBER TRATMENT EFFECT ON TITANIUM/BONE INTERFACES 35

4.1 Summary 35

4.2 Background 35

4.3 Materials and Methods 38

4.3.1 Materials 38

4.3.2 Specimen design 38

4.3.3 Preparation of Ti samples 39

4.3.3.1 Control samples 39

4.3.3.2 Groove samples 39

4.3.3.3 Groove-NFM samples 40

4.4 Animal surgery 40

4.4.1 Pull out tension tests 42

4.4.2 Statistical Analysis 42

4.5 Results 42

4.5.1 Nanofiber characteristics 42

4.5.2 Ti sample characteristics 43

4.5.3 General observations of animals 44

4.5.4 Mechanical testing 44

4.6 Conclusion 45

4.7 Figures 46

4.8 Tables 52

5 IN VIVO EVALUATION OF THE MgO NANOPARTICLES EFFECT ON TITANIUM/CEMENT INTERFACES 53

5.1 Summary 53

5.2 Background and Significance 53

5.3 Material and Method 54

5.4 Results and discussion 54

5.5 Conclusions 55

5.6 Figures 56

6 DESIGN AND EVALUATION OF A COMPOSITE HYDROGEL SCAFFOLD AS A BONE GRAFT 57

6.1 Summary 57

6.2 Specification and Background 57

6.3 Material and Method 58

6.4 Results 59

6.5 Conclusions 60

6.6 Figures 61

7 DESIGN AND EVALUATION OF ELECTROSPIN FIBER ANCHORED INTERVERTEBRAL DISC IMPLANT 64

7.1 Summary 64

7.2 Specification and Background 64

7.3 Material and Method 65

7.3.1 Introduction 65

7.3.2 Fabrication steps 66

7.3.2.1 Production of nucleus pulposus (NP) disc 66

(a) NP disc Material type 1: Silicone 66

(b) NP disc Material type 2: PEGDA 67

(c) NP disc Material type 3: PCL/PEGDA composite disc 68

7.3.2.2 Coating on top and circumferential surface of the NP disc by random fiber 68

(a) Coating on the bottom surface of the NP disc by random fiber. 69

(b) Coating on circumferential surface of the disc by aligned fiber 69

7.3.2.3 Production of Engineered IVD 70

(a) Silicone IVD (non-tissue engineered IVD) 70

(b) PEGDA based tissue engineered IVD 70

(c) PCL/PEGDA composite tissue engineered IVD 70

7.3.3 Mechanical tests on silicone EIVD 71

7.3.3.1 Sample preparation 71

7.3.3.2 Compressive and Rheological tests 71

7.3.4 *Ex vivo* mechanical tests of silicone EIVD using rabbit caudal spine 71

7.3.4.1 Sample preparation 71

7.3.4.2 Mechanical testing 72

7.4 Results 72

7.4.1 Mechanical tests on silicone EIVD 72

7.4.2 Ex vivo mechanical tests of silicone EIVD using rabbit caudal spine 73

7.5 Conclusions 73

7.6 Figures 74

7.7 Tables 80

8 CONCLUSION AND FUTURE WORKS 81

8.1 Conclusions 81

8.2 Future works 83

LIST OF FIGURES

Figure 1-1 Schematic of electrospinning set up 7

Figure 1-2 Flowchart of the study outline 8

Figure 2-1 (a)Custom-made polishing setup using Buehler IsoMet low speed saw.(b) Disc used for polishing. 18

Figure 2-2 (a) Schematic presentation of laser peening treatment location and (b) a peen treated sample 18

Figure 2-3 Static tests setup on universal testing machine 18

Figure 2-4 Measurement of the cement height by cutting cement holding cup into half using the band saw machine 19

Figure 2-5 Laser-peened Ti samples. (left) Control and (right) peen-treated sample set . 19

Figure 2-6 (top) Confocal area scan (876.55 µm ×659.83 µm) image of laser peen-treated sample. (bottom) Confocal Z scan (130 µm) to find the depth profile along a vertical line indicated in top figure. 19

Figure 2-7 Load–displacement curves of three samples during the static tests on 20

Figure 2-8 Bar diagram of the variation of fracture strength of control samples (Ti) with peen-treated samples. Notes: Data presented as mean ±standard error of mean; n=3 for control and laser peen-treated samples. *P<0.05 (compared to control). 20

Figure 3-1 (a) Schematic of plasma setup showing the top and bottom plates separated by a distance, d and (b) Glow discharge Plasma 31

Figure 3-2 (a) Fabricated holder for static test, and (b) Static tests setup on UTM 31

Figure 3-3 (a) Topography and (b) intensity layers confocal microscope images of a Ti sample. (c) Topography and (d) intensity layers confocal microscope images of a plasma treated Ti. 32

Figure 3-4 Load-displacement curves of 3 samples during the static tests on Ti-cement interfaces: (a) control and (b) plasma treated samples. 32

Figure 3-5 Bar diagram of the variation of fracture strength of control samples (Ti) with plasma treated samples, Data presented as means ± standard error of mean; n=3 for control; n=4 for the plasma treated samples. Note: *p<0.05 (compared to PMMA) 33

Figure 4-1. Flowchart showing the steps of determining fracture strength of Ti samples. 46

Figure 4-2. Schematic representation of longitudinal section images of a (a) control, (b) groove, and (c) groove-NFM samples 47

Figure 4-3. Polishing of Ti wire using a drill machine chuck and gripper 47

Figure 4-4. Micron depth grooving on the circumference of a Ti wire using Buehler diamond saw blade check and gripper. The gripper is holding a motor in which the shaft of the motor is secured with the implant. 47

Figure 4-5.Schematic representation of coating groove Ti samples by aligned electrospun nanofiber using an electrospin process. 48

Figure 4-6. (a) X-ray image of femur after surgery, (b) a test sample after cleaning the soft tissue around the implant after euthanasia, (c) dissection of a sample using the Buehler saw machine, (d) a sample for mechanical and histological tests after trimming. 48

Figure 4-7. Mechanical tests steps:(a) holding samples at the top gripper and pouring cement into the sample holder, (b) sealing the samples in the cement and curing the cement for an hour, and (c) quasi-static pull out tension test of a cured sample. Figure shows a sample after breakage. 48

Figure 4-8. Fabricated uni-direction nanofiber between two parallel wires 49

Figure 4-9**.** Scanning microscope image of the aligned PCL nanofiber on a carbon type at (a) 800 X and (b) 1500 X magnifications. Figure (b) shows the diameter of the fiber and the distance between the fibers. 49

Figure 4-10. A fabricated (a) control, (b) groove, and (c) groove-NFM samples. 49

Figure 4-11. (a) Attachment of CG-PCL NFM coating after *in vitro* cell culture on Ti plate after 3 weeks of cell culture, and (b) Attachment of CG-PCL NFM coating after *in vivo* implantation of Ti wire after 8 weeks. 50

Figure 4-12. Load vs displacement plot of a control, groove, and groove with NFM samples. 50

Figure 4-13. Push-out test results (in MPa) of different titanium samples after 8 weeks of implantation. Bars represent means ± SD (n = 6). * represents statistical significant results compared to control samples for *p value* = 0.05. 51

Figure 5-1 CT scan image of cemented implant 56

Figure 5-2 Comparison of fracture strength between with and without MgO added cemented samples. 56

Figure 6-1 Schematic representation of the process for creating a composite scaffold made with 4 layers of PCL ENF membrane and 3 layers of PEGDA hydrogel 61

Figure 6-2 UV photo polymerization unit used for curing PEGDA hydrogel 61

Figure 6-3 Fabricated 10 mm diameter and 1.5 mm thickness composite hydrogel on the mold. 61

Figure 6-4 Separated composite scaffolds from the mold:(a) PEGDA and (b) PCL-PEGDA. Topographical images of composite scaffolds using SEM: (c) PEGDA and (d) PCL-PEGDA 62

Figure 6-5 Evex mechanical test setup for compression tests on scaffold 62

Figure 6-6 Load vs. displacement curves for scaffolds 63

Figure 7-1 Schematic representation of different components of IVD..... 74

Figure 7-2: Silicone Synthesis and Disc Procedure 75

Figure 7-3 PEGDA Synthesis and Disc Procedure 76

Figure 7-4 (a) Curing of PEGDA solution in a custom made plastic syringe at the UV chamber and (b) produced PEGDA disc that was pushed out from the plastic syringe chamber 76

Figure 7-5 Coating of NP disc in top and circumferential sides by random fibers 77

Figure 7-6 Coating of NP disc by random fibers in the side where there is no existence of fiber coating 77

Figure 7-7 Coating of NP disc by random fibers 78

Figure 7-8 Components of the engineered IVD that mimic the architecture of natural IVD. 78

Figure 7-9 Production of angle ply structure on the circumference of NP disc. 78

Figure 7-10 Preparation of PEGDA based tissue engineered IVD 79

Figure 7-11 PEGDA IVD in PBS solution at 38 degree centigrade in an incubator. 79

Figure 7-12 (a) CT scan image of a rabbit tail, (b) IVD implantation on rabbit tail, (c) sutured tail having IVD implant, (d) sample in a Test Resource UTM, and (e) load-displacement curve of native and implanted samples. 79

LIST OF TABLES

Table 2-1Difference of roughness between control and laser peen-treated..... 21

Table 2-2 Summary statistics for static tests experimental data by group..... 21

Table 3-1 Some specific parameters of surface 34

Table 3-2 Summary statistics for static tests experimental data by group..... 34

Table 4-1. Geometric parameters of Ti samples. The values are given as means ± =SEM (n = 6 each). * Significantly greater than control (P <0.05); †significantly greater than groove. 52

Table 7-1 Difference between viscoelastic properties between silicone gel and human NP materials. 80

LIST OF ABBREVIATION

PMMA: Polymethylmethacrylate

PCL : Polycaprolacton

MgO: Magnesium oxide

CG: Collagen

PEGDA : Polyethylene Glycol Diacrylate

IVD: Intervertebral disc

Ti: Titanium

MMA: Methylmethacrylate

NFM: Nanofiber mesh

ENF: Electrospun nanofiber

NP: Nucleus pulposus

Chapter 1

INTRODUCTION

1.1 Electrospinning

Eloctrospinning is a simple method and popular technique for the fabrication of macro to nanofibers. In the electrospinnig process, a high voltage supplier is used to create an electrical field, a pump syringe for injection of a molten polymer, and a collector for gathering the fibers. In the last two decade, produce nanofiber by the electrospinning process has increased much consideration because it is an effective method to make ultrafine fibers with diameter in the range from several micrometers to tens of nanometers [1, 2]. This method is an economical and simple way for producing polymer nanofibers with diameters ranging typically between 50 and 500 nanometer [3].

In the electrospinning process, the main components are: a high voltage supplier, pump injection, collector, small diameter tube, syringe, and needle. In this process after preparing molten polymer, charge the solution in the syringe and set on the injection pump, a high voltage source is used to create an electrical field. Positive pole connects to the needle and the collector is the negative pole (grounded). Schematic of electrospinnig set up is shown in Figure 1-1.

1.2 Implant fixation technique

The big challenges in orthopedic and orthodontic are the implant loosing or the breakage at the implantation sits and improve the bonding between the interface materials. The purpose of the thesis is to improve the union of implant with bone for both cemented and cementless fixation techniques. Cemented fixation is more common for osteoporotic bone, where the bone cement is used to hold the implant in place. For healthy bone, bone can grow into the surface of the implant by osseointegration. Cementless fixation is more expensive and has less long-term stability when compared to cemented fixation. Furthermore, bone cuts require a perfect match with the component for cementless

fixation. This thesis develops techniques for fixation of Ti implants for cemented and cementless surgeries.

There are numerous commercially available tissue engineering scaffolds, however most of the scaffolds have limited mechanical and biological capabilities, particularly scaffolds for bone grafting and intervertebral disc (IVD) materials. This is the reason for the constantly growing interest in the bone grafting and IVD materials. This thesis develops novel materials for bone grafting and intervertebral disc (IVD) applications..

1.3 Implants investigated in this study

1.3.1 Titanium

Metals are extensively used as implants for hard tissue repair. Titanium based alloy have been mostly used in orthopedic and orthodontic surgeries as implants because of their strong mechanical, chemical, and biological properties. A Titanium based alloy have been widely used in orthopedic and orthodontic surgeries as implants because of their strong mechanical, chemical (corrosion resistance), and biological properties and biocompatibility [4-6]. The dissolution of Ti into body is very trivial because Ti metal surface can spontaneously form a stable and inert layer of titanium dioxide (TiO_2), which will prevent Ti metal from reacting with body fluid [7]. Ti has its excellent biocompatibility (high corrosion resistance, low ion-formation tendency, low level of electronic conductivity, etc.) mostly owing to this oxide layer. Comparing to commercial pure Ti, Ti alloys such as Ti-6Al-4V exhibit solid solution hardening and have lower fusion temperatures and better ductility [8]. Among the various Ti alloys, Ti-6Al-4V, which was used in this study, is the most widely used as implant because of its better physical and mechanical properties in comparison to pure Ti.

1.3.2 Bone Cement

Bone cement is used in various orthopedic surgeries. Among the many potential bone cement materials, polymethylmethacrylate (PMMA) bone cement has been successfully used in orthopedic surgeries mostly because of its strong mechanical

bonding with implant. PMMA bone cements are provided as two-component materials, a powder (PMMA beads) and a liquid (MMA monomer). These two components are mixed at 2:1 ratio and polymerization occurs. The current most commercially available PMMA bone cements are Cobalt (Biomet, Inc.), Simplex (Stryker, Inc.), and Palacos (Heraeus Company), and Veterinary bone cement (Bio Medtrix, LLC). However, several drawbacks associated with PMMA bone cement limit its efficacy. For example, PMMA cement adheres inadequately to the bone surfaces (no bioactivity) [9], has a high exothermic reaction temperature [10] and exhibits monomer toxicity [11]. Particularly, enough bonding strength of cement with the implant and bone is required for the design of optimal bone cement. Whereas, increasing the bonding strength of implant-cement interfaces is imperative. It may be accomplished by increasing the surface interlock of implant-cement or bone-cement interfaces through enlarging the surface roughness of the cement mantle or the implant surface. The typical bone cement used in this study was Cobalt HV PMMA bone cement and Veterinary bone cement.

1.3.3 PEGDA

Polyethylene Glycol Diacrylate (PEGDA) is 3D networked structures that can be manufactured easily to allow for cell growth at higher depth using photolithograph process. Photolithography is a process which is commonly used in microfabrication to produce the desired scaffolds with a high level of detail and precision. It has been found to be a valid method to manufacture multiple-layer scaffolds for allowing the constructions of channels within the scaffold to better distribute nutrients to the cells. PEGDA tissue scaffolds having thickness higher than 1 mm were shown to have limited applications as a three-dimensional cell culture device due to the inability of cells to survive within the scaffolds. Without access to adequate nutrients, cells placed deep within the PEGDA tissue construct having thickness higher than 1 mm die out, leading to nonuniform tissue regeneration. One of the goals of this thesis is to improve the biological performances of PEGDA scaffold by incorporating nanofiber.

1.3.4 Silicone

Silicone is a non-hydrogel based synthetic polymer. Silicone has material properties that make it ideal for many applications in the biomedical fields. It is hydrophobic nature, moldable, low surface tension, and good biocompatibility. In this thesis, silicone has been used as gel as a replacement of nucleus pulpous for degenerated intervertebral disc.

1.4 Modification of implant surface

1.4.1 Peen treatment

Peening is one of the most frequently used treatments for obtaining a rough surface of an orthopedic or orthodontic implant [12]. Shot peening is used to bombard implant surfaces with chemically stable materials that will not negatively affect the biological behavior of the implant[13]. Laser peening, on the other hand, is an engineered process that uses beneficial residual stresses by spot grooving to provide strong, reliable products.

1.4.2 Plasma treatment

There are few techniques for plasma-surface modification such as plasma spray, plasma immersion ion deposition which are recognized to be economic and effective, have already been widely applied in modification of biomedical implants. There are sophisticated thin film of attaining plasma nitride is by a simple DC glow discharge nitrogen plasma treatment. The unique advantage of plasma modification over the other methods is the ability of selectively enhancing surface properties (within several hundred nanometers), whereas the bulk contributions remain unchanged[14].

1.4.3 Nanofiber and nanoparticles

Nanofiber and nanoparticles treatment are varieties can modify the surface of implant and increase mechanical interlock, surface energy, and osseointegration of titanium surface that lead to improve in vitro and in vivo mechanical integration of Ti/bone or Ti/cement interfaces. Treatment by nanofiber and nanoparticles are simple,

scalable, low-cost, and supplementary surface treatment technique. Such treatment can applied on Ti surface without impressively affecting other implant factor such as plasma and peening treatment.

1.5 Motivation and goals

The motivation of this thesis was to evaluate three nanotopographical modifications techniques; peening, plasma, and electrospun nanofiber to improve the mechanical and biological functions of metallic and polymeric implants. The goals were to measure the effect of laser peening, plasma nitridation and electrospun nanofiber coating techniques on the mechanical and biological functions of titanium implant. In addition, the goals were to design polyethylene Glycol Diacrylate (PEGDA) and silicone based tissue engineering scaffold as bone graft and intervertebral disc implants using electrospun nanofiber coating techniques.

1.6 Objectives

The objectives of this thesis are: 1) Effect of electrospun fiber material on the Ti/PMMA cement interface. 2) The effect of laser peening treatment on titanium implant.3) the effect of Plasm-nitride treatment on titanium implants. 4) Evaluation of the electrospin fiber treatment on titanium/bone interfaces 5) Evaluation of the electrospin fiber treatment effect on titanium/cement interfaces. 6) Design and evaluation of electrospin fiber based intervertebral disc implant 7) Design and evaluation of electrospin fiber anchored intervertebral disc implant

1.7 Organization of the thesis

Figure 1-2 shows the flowchart of the study outline. This thesis contains eight chapters. Chapter 1 is the introduction of the thesis. In Chapter 2 laser peening treatment on Ti surface was conducted. In this chapter also explained about the kind of peening techniques, polishing process, electrospinning process. Chapter 3 also explain about the effect of Titanium Nitrogen plasma treatment of Ti on the static test also measured the surface morphology and surface hardness. In chapter 4, static test and fatigue test of Ti-

bone interface was conducted (in vivo). Chapter 5, experimental static test of Ti-cement and Ti-bone of rabbit was conducted. In this chapter also showed the process for preparing samples for surgery and all steps after surgery for preparing samples for test. Also, evaluation of the electrospun fiber treatment effect on titanium/cement interfaces was conducted. In chapter 6, design of electrospun fiber based intervertebral disc implant and determined the compression test for samples. In the chapter 7, Develop 3D tissue engineering scaffold using an electrospun fiber process and fabrication of a hydrogel-electrospun fiber mat composite scaffold were conducted. In chapter, 8 conclusion and future work is explained.

1.8 Figures

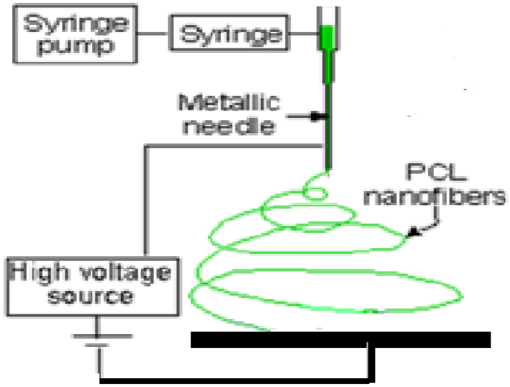

Figure 1-1 Schematic of electrospinning set up

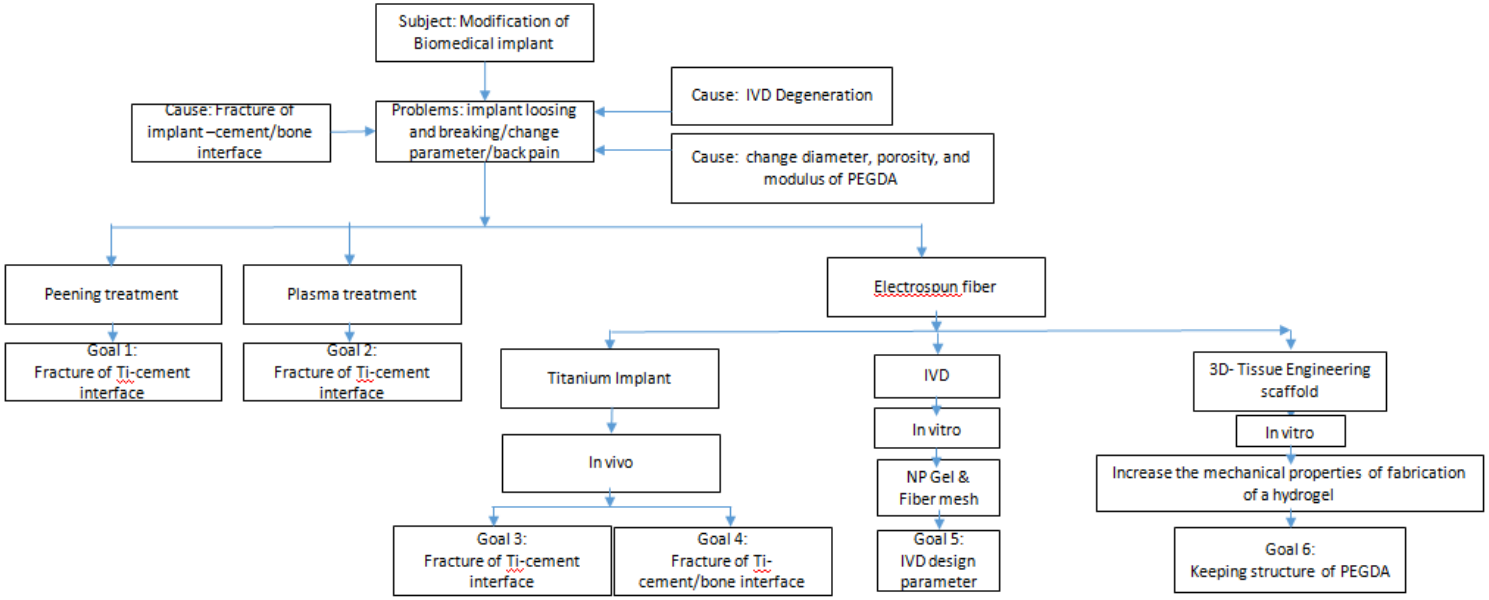

Figure 1-2 Flowchart of the study outline

CHAPTER 2

PEEN TREATMENT ON TITANIUM IMPLANT

2.1 Summary

Implant failure due to poor integration of the implant with the surrounding biomaterial is a common problem in various orthopedic and orthodontic surgeries. Implant fixation mostly depends upon the implant surface topography. Micro to nano size circular-shaped groove architecture with adequate surface roughness can enhance the mechanical interlock and osseointegration of an implant with the host tissue and solve its poor fixation problem. Such groove architecture can be created on a titanium (Ti) alloy implant by laser peening treatment. Laser peening produces deep, residual compressive stresses in the surfaces of metal parts, delivering increased fatigue life and damage tolerance. The scientific novelty of this study is the controlled deposition of circular-shaped rough spot groove using laser peening technique and understanding the effect of the treatment techniques for improving the implant surface properties. The hypothesis of this study was that implant surface grooves created by controlled laser peen treatment can improve the mechanical responses of the implant with the adjoining biomaterial. The objective of this study was to measure how the controlled laser-peened groove architecture on Ti influences bonding strength with bone cement. This study determined the surface roughness and morphology of the peen- treated Ti. Finally, this study measured the fracture strength between each kind of Ti samples and bone cement under static loading. This study found that laser peen treatment on Ti significantly changed the surface architecture of the Ti, which led to enhanced differentiation on Ti implants and fracture strength of Ti–bone cement interfaces compared with values of untreated Ti samples. Therefore, the laser peen treatment method has the potential to improve the biomechanical functions of Ti implants.

2.1 Background and specification

2.1.1 Introduction

The use of fixed, cemented implants was an innovation that provided more long-term stability than uncemented implants; however, clinical loosening of the cemented replacements has been reported. In USA,~600,000 cases of poor union and 100,000 cases of nonunion of implants with the surrounding tissue are reported every year[15]. Many manufacturers have recalled their hip implants (including Johnson & Johnson [New Brunswick, NJ, USA], DePuy [West Chester, PA, USA], and Zimmer Durom [Warsaw, IN, USA])[16]. A patient's age, sex, weight, diagnosis, activity level, surgery condition, and implant choice influence the longevity of the device. The primary cause of failure of cemented joint replacements is aseptic loosening of the components, which may arise from mechanical failure of the cement mantle surrounding the implant[17]. It has been pointed out that the debonding of stem–cement interface enables gapping and sliding between the stem and the cement[18, 19].

A wide variety of surface modification techniques have developed with the aim of solving the implant failure problem. Many papers reported the nanoscience techniques, such as plasma sintering, plasma nitridation, for obtaining a rough surface on an orthopedic or orthodontic implant [20, 21]. The augmentation of the surface roughness or surface energy allows for developing mechanical interlock of the implant and bone cement interface which can improve the bonding characteristics of the implant–cement interface[22]. Hosein et al[23]pointed out that circumferential-grooved stems offered improved stability under compression relative to the smooth stems. It has been revealed that porous coating of the femoral stems dramatically improved push-out strengths and fatigue properties of the stem–cement interface through increasing surface roughness [24]. In addition, various implant coatings, including titanium dioxide with integrated copper ions, plasma polymerized allylamine, calcium phosphate, and titanium nitride have been investigated regarding the adhesion strength and wear resistance [25]. Shot peening is one of the most frequently used treatments for obtaining a rough surface for an

orthopedic or orthodontic implant [12]. Shot peening is used to bombard implant surfaces with chemically stable materials that will not negatively affect the biological behavior of the implant[26].

Laser peening, on the other hand, is an engineered process that uses beneficial residual stresses by spot grooving to provide strong, reliable products. Laser peening has been shown to increase service lifetimes of components by more than ten times that of the as-manufactured condition, and that of parts treated with other conventional surface enhancement methods [27, 28]. Shot or laser peening induces a residual stress layer in the treated material because of the local plastic deformation of the metal [31]. Although the variables of shot blasting are not exhaustively controlled, as opposed to laser peening, the stressed superficial layer is in compression and, consequently, an increase in the fatigue resistance of the peen-treated implant is expected. In the case of laser peening, the rapid rise of pressure generated at the surface of the workpiece by the high energy laser pulse creates a shockwave in the part. The pressure pulse typically has a length of 2–2.5 times that of the laser pulse [32]. As the shockwave travels into the object, some of the energy of the wave is absorbed by the plastic deformation and beneficial residual stress accumulates in the object area. The indented surface area, dislocations, and nano crystallization, which are typically instigated onto the implant surface by laser peening, are chemically stable materials that should not stimulate a negative response of the biological behavior of the implant. Rather the implant surface grooves created by laser peening may provide favorable depth for cell adhesion and enhance mechanical interlock between the implant and the cement, which will improve the union between the implant and the cement. The influence of the laser-peened treatment on the cell adhesion and fracture strength of Ti–cement was studied in this research.

2.1.2 Research questions

This study was conducted based on these questions: 1) is there a significant change in the surface architecture of the Ti by use the laser peen treatment on Ti? Is there a significant different in mechanical performances between untreated Ti (control)

and laser peen treated samples? Is this method has the potential to improve the biomechanical function of Ti implants?

2.1.3 Scope of work

The scope of work for this study was: 1) to determine the optimal surface roughness and morphology of the peen- treated Ti 2) to measure the fracture strength between each kind of Ti samples and bone cement under static loading.

2.2 Material and method

2.2.1 Sample Preparation

This study used titanium alloy, 6Al-4V ELI as the titanium implant. Among the various Ti alloys, 6Al-4V ELI was used in this study because of its better physical and mechanical properties in comparison to pure Ti [8]. The 6Al-4V ELI titanium alloy round rod was referred in this study as the Ti rod. Two sets of round 6Al-4V ELI Ti rods (ASTM B 348 standard, grade 23, ultimate tensile strength 125 ksi, Yeild Strength 115 Ksi) having same diameter (9.565 mm), but different lengths (8 mm and 76 mm) were purchased from Titanium Metal Supply, Inc., Poway, CA. In this study, 9.565 mm diameter and 8 mm height Ti rod was referred as sample set 1, whereas 9.565 mm diameter and 76 mm height peen treated Ti rod was referred as sample set 2. The above two sizes of Ti rods without laser peening was referred as control. Sample set 1 Ti rods were used for cell proliferation and differentiation tests on the Ti. Sample set 2 Ti rods were used for mechanical tests on the Ti-PMMA bone cement samples.

Among the many potential bone cement materials, polymethylmethacrylate (PMMA) bone cement has been successfully used in orthopedic surgeries mostly because of its strong mechanical bonding with implant. PMMA bone cements are provided as two-component materials, a powder (PMMA beads) and a liquid (MMA monomer). These two components are mixed at 2:1 ratio and polymerization occurs. Cobalt™ HV bone cement (Biomet Inc., Warsaw, IN) was used as the bone cement.

2.2.2 Polishing protocol

Both control and laser peened Ti samples were polished to have uniform surface morphology for mechanical tests. Three polishing steps were followed for the circumferential polishing on the Ti rods. A custom made polishing system ((Figure 2-1 (a)) based on Buehler Isomet low speed cutter were used for 12 mm circumferential polishing from an edge. The saw blades of Isomet low speed cutter were replaced by a custom made round disc ((Figure 2-1(b)). The polishing pads (CarbiMet 2, Ultra Pad, and micro cloth) were secured around the circumference of the round disc. Sample set 2 Ti rod samples were fixed with the shaft of a DC motor in a custom made holder. The rotations of polish disc and Ti rod were controlled by the Buehler Isomet cutter speed and DC motor voltage, respectively. The rotational friction between Ti rod and round disc was used to polish uniformly the circumference of the Ti rod. For all three sets polishing, Buehler Isomet cutter speed was set to 6 and DC motor voltage was set to 6.8V.

2.2.3 Laser peening treatment on Ti

Laser peening was conducted on samples at the locations as schematically shown in Figure 2-2 using Procudo™ laser peening systems (LSP Technologies, Inc., Dublin, OH, USA). LSP Technologies, Inc. is an AS9100 certified provider of laser peening. Ti rods were polished circumferentially up to 10 mm from an edge. Samples had ten separate bands of treatment applied to each sample at points 30 degrees around the circumference (12 points per band). A custom machine control program was developed for the laser peening procedures. All Ti rods (control and peen-treated) were sterilized by autoclaving for further experiments.

2.2.4 Surface roughness and morphology

Surface morphology is an important parameter that plays a significant role in implant-cement, and implant-bone adhesion. So, the influence of laser peen treatment to surface morphology was evaluated by a Leica DCM8 surface metrology instrument using 20x

bright field confocal control condition. A line scan was conducted both samples. Roughness and depth profile along the scanned line were compared.

2.2.5 Mechanical tests on Ti/cement samples

Sample sets control and laser peen-treated Ti rods were used to find the effect of laser peen treatments on the bonding strength between the Ti rods and cement under static loading. A Test Resources (Shakopee, MN, USA) universal testing machine (UTM) was used for the mechanical tests. The top gripper of the UTM held the Ti rods (Figure 2-3). A 3D printed (Dimension elite 3D printer; Stratasys, Edina, MN, USA) cylindrical-shaped cement holding cup was fabricated to encapsulate the Ti rod with ~2.8 mm thick and 12 mm height PMMA cement layer. The cup was placed at the center of the bottom base of the UTM with the help of another 3D printed plate, referred in the Figure 2-3 as cement press plate. The plate has a tube extruded from the center of the plate. The dimension of the inside and outside diameter of the tube was such that the Ti rod and cup fit within the tube. The plate slid onto the Ti rod. The Ti rod with the plate was jogged down until the Ti rod touched the bottom surface of the cup.

According to Cobalt ^{HV} bone cement manufacturer package recommendations, PMMA cement was prepared by hand mixing 2.2 grams of PMMA powder with 1.1 ml of methyl methacrylate (MMA) monomer using powder: monomer ratio of 2:1. PMMA cement paste was poured into the gap between the Ti and cup. The plate was pressed by hand to encapsulate the bottom end of the Ti rod with cement. The plate was bolted with the bottom gripper of the UTM. After curing the cement for 15 minutes, static tests were conducted at strain rate 0.05 mm/sec on the sample to find fracture strength of the Ti/PMMA samples. Load and displacement data during the test were recorded. The maximum pull out force, F, was determined from the recorded data. The cup was cut in half to measure the height of the cement layer of the Ti/PMMA samples (Figure 2-4). The average cement layer height, L, was measured. Fracture strength of the Ti/PMMA interface was calculated by dividing the maximum pull out force by the surface area of the implant in contact with the cement (πDL), where D is the diameter of the Ti rod.

2.3 Result

Figure 2-5 shows the stereomicroscope images of a control and laser peen-treated sample sets used for the mechanical test. A clear difference of surface topography between the control and laser peen-treated samples can be seen from the images. Laser-peened indentation sites were clearly visible for both kinds of samples. Confocal laser microscopic image of a peen-treated sample used for cell studies shows a clear topographical difference between non-peen-treated and peen- treated sites (Figure 2-6). The depth (z-axis height) line profile along a vertical path that covered both non-peen-treated and peen-treated sites (Figure 2-6) showed the quantitative difference of surface indentation depth between the sites. Figure 2-6 shows a difference of 1.49 µm in the average depth values between non-peen-treated and peen-treated sites for same linear distance (190.30 µm). In addition, the surface roughness of laser-peened samples was found to be higher compared to control samples (Table 2-1). The comparison of the load–displacement plots of a control and peen-treated specimen is shown in Figure 2-7. A sudden increment of load was observed for all specimens at the initial stage. Such high initial load was higher for peen- treated samples compared to the control samples. After the high initial load, the slope of the load versus displacement value for all control samples was higher at the initial stage than the slope at failure stage (1.66 vs 1.36 N/mm, 1.13 vs 1.06 N/mm, and 1.69 vs 1.04 N/mm). In contrast, after the high initial load, the slope of the load versus displacement value for all laser peen-treated samples was lower at the initial stage than the slope at failure stage (1.2 vs 2.1 N/mm, 2.64 vs 3.12 N/mm, and 1.11 vs 1.24 N/mm). This result occurs due to the surface topographical variation between the control and laser peen-treated samples. The increment of load with displacement behaved linear until the onset of cracking, which is observed in the figure by the nonlinearity (fracture initiation) point of the load–displacement curve. Also, Figure 2-8 shows that the peen-treated specimen required more fracture load than the control specimen. Results show that the amount of displacement before the initiation of crack at the interface is different between control and peen-treated samples. The values of fracture strength of both samples were calculated. The specimen static tests,

experimental parameters, and mean fracture strengths for the control and peen-treated groups are displayed in Figure 2-8 and Table 2-2. There was a significant difference in the mean fracture strengths of the groups (t=4.24, P=0.036). Since higher fracture strength of a biomaterial interface means better union of the interface, therefore, the previous results suggested that peen treatment has a positive influence on the union between Ti and cement interfaces.

2.4 Discussion

Laser peening treatment on a Ti alloy demonstrated better cell adhesion and bonding strength between the metal and cement compared to control. Higher surface roughness, surface energy, pores, dislocation arrangement, and nano crystallization are some of the potential causes for the mechanical improvements. Surface roughness measurements showed that the roughness achieved by polishing and subsequent laser peening is much higher than surface roughness achievable by simple polishing (Table 2-1). Surface dislocation arrangement and nanocrystallization triggered by laser peening can effectively enhance surface mechanical properties such as elastic modulus and wear resistance. Khandaker et al. previous studies found that, the elastic modulus of cement and wear resistance of an implant due to nanofiber coating on the implant controls the bonding strength between the implant and the cement.25,30 Thus, laser peen-created surface dislocation arrangement and nano crystallization on Ti-based alloys may affect the bonding strength between Ti and cement.

The limitation of the study was that the area topography scan was conducted using confocal laser microscope on only one control and peen-treated samples to evaluate the topographical differences between the samples. The reason for not using the multiple samples was that laser peen-treated samples create distinct circular textures, which are not present in control samples. Also line topography scan was conducted using confocal laser microscope only one peen-treated sample to evaluate the topographical differences between the non- peen and peen-treated sites. The reason for using one site for evaluation was that each of the laser-peened sites was created by same amount of energy

laser pulse applied to each of the sites. Therefore, we assumed that all laser-peened sites should have the same depth characteristics.

2.5 Conclusion

The objectives of the study were the evaluation of the surface morphology and interface fracture strength of Ti due to laser peen treatment on a Ti implant. This study concluded that the laser peen treatment significantly changed the nano architecture of Ti samples, which lead to mechanical stability of Ti with PMMA bone cement. These studies concluded that laser peen treatment on the Ti alloy can potentially improve the union between titanium–cement interfaces.

2.6 Figures

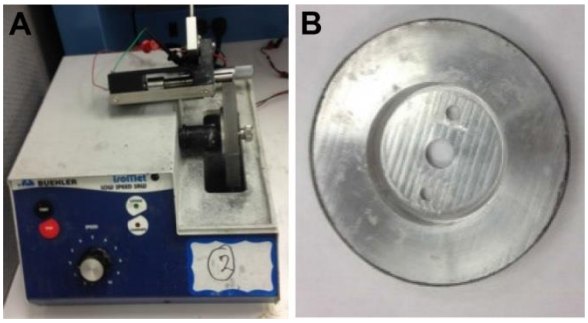

Figure 2-1 (a)Custom-made polishing setup using Buehler IsoMet low speed saw.(b) Disc used for polishing.

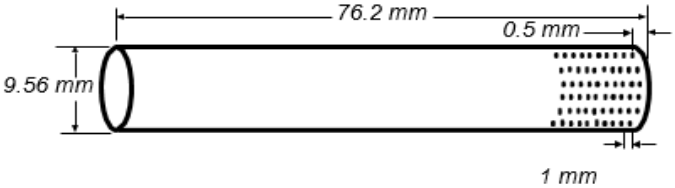

(a)

(b)

Figure 2-2 (a) Schematic presentation of laser peening treatment location and (b) a peen treated sample

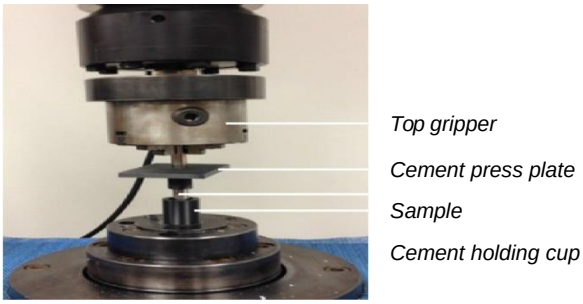

Figure 2-3 Static tests setup on universal testing machine

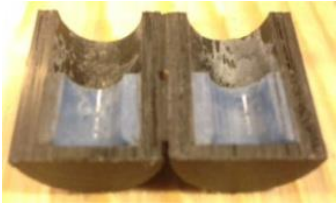

Figure 2-4 Measurement of the cement height by cutting cement holding cup into half using the band saw machine.

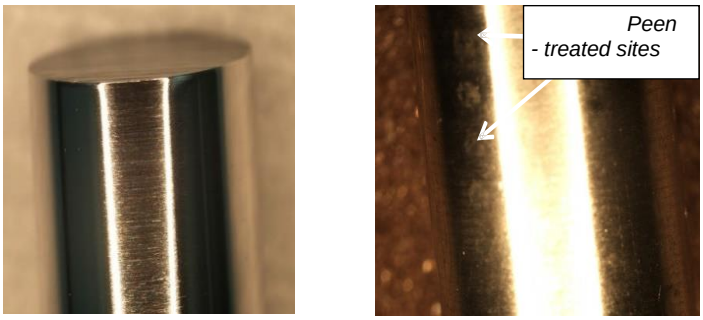

Figure 2-5 Laser-peened Ti samples. (left) Control and (right) peen-treated sample set

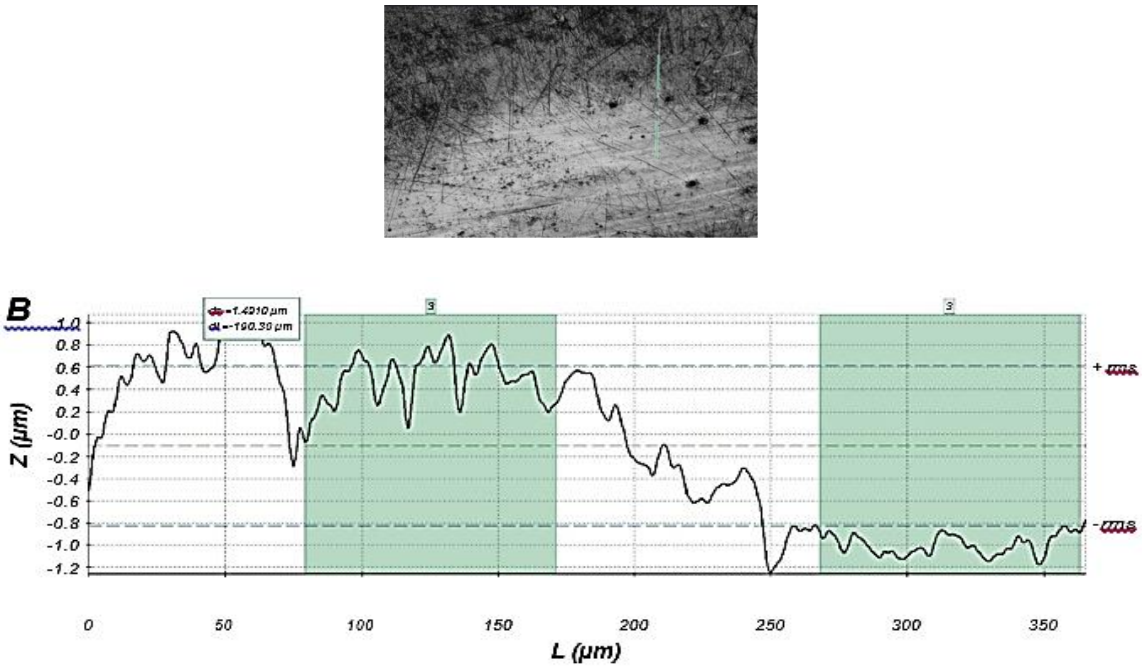

Figure 2-6 (top) Confocal area scan (876.55 µm ×659.83 µm) image of laser peen-treated sample. (bottom) Confocal Z scan (130 µm) to find the depth profile along a vertical line indicated in top figure.

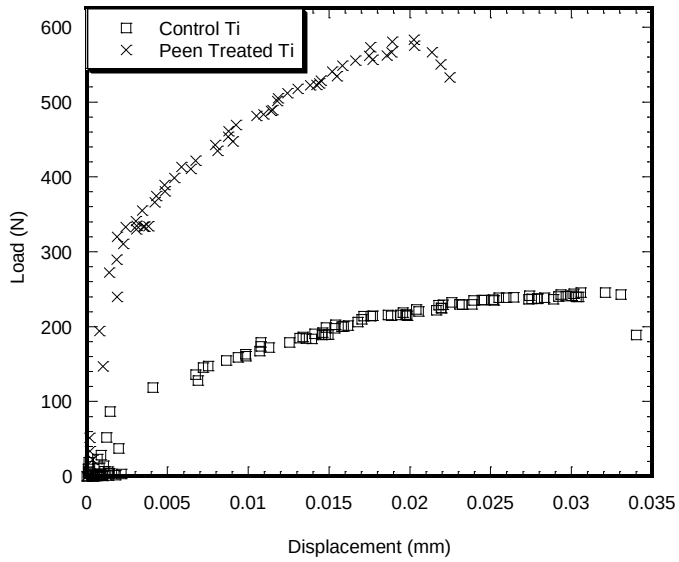

Figure 2-7 Load–displacement curves of three samples during the static tests on Ti–cement interfaces.

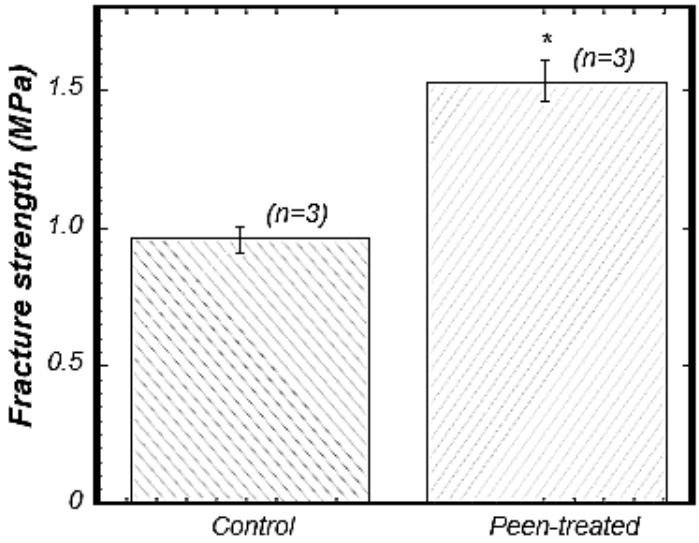

Figure 2-8 Bar diagram of the variation of fracture strength of control samples (Ti) with peen-treated samples. Notes: Data presented as mean ±standard error of mean; n=3 for control and laser peen-treated samples. *P<0.05 (compared to control).

2.7 Tables

Table 2-1Difference of roughness between control and laser peen-treated

Descriptions	Control	Peen treated
Profile length	178.09 µm	365.13 µm
R_a	0.10 µm	0.66 µm
R_q	0.13 µm	0.72 µm
R_p	0.28 µm	1.18 µm
R_v	0.35 µm	1.15 µm
R_z	0.63 µm	2.33 µm

Table 2-2 Summary statistics for static tests experimental data by group

Parameters descriptions	Control	Peen treated
No of samples tested	3	3
Height of implant-cement interface	10.23 ± 0.18	11.48 ± 0.46
Contact Area	307.34 ± 5.47	338.76 ± 13.76
Fracture load	329.21 ± 41.05	527.01 ± 39.77
Fracture strength	1.05 ± 0.14	1.54 ± 0.18

CHAPTER 3

DIRECT CURRENT GLOW DISCHARGE NITROGEN PLASMA TREATMENT ON TITANIUM IMPLANT

3.1Summary

Titanium (Ti) alloys have been widely used in orthopedics and orthodontic surgeries as implants because of their beneficial chemical, mechanical, and biological properties. Improvement of these properties of a Ti alloy, Ti-6Al-4V Eli, is possible by the use of plasma nitriding treatment on the Ti alloy. The novelty of this study is the evaluation of a DC glow discharge nitrogen plasma treatment method on the surface, mechanical properties of Ti alloy. Specifically, this study measured the roughness, hardness of plasma nitride treated Ti-6Al-4V Eli as well as determined the effect of plasma treatment on the fracture strength between the Ti alloy and bone clement. This study hypothesized that DC glow discharge nitrogen plasma treatment may alter the surface chemical and mechanical states of the Ti alloy that may influence the fracture strength of implant/cement interfaces under static load. This study found that plasma nitride treatment on Ti alloy does not have effect on the roughness and biocompatibility (P value > 0.5), but significantly effect on the hardness and fracture strength of Ti-bone cement interfaces compared to those values of untreated Ti samples (P value < 0.5). Therefore, the DC glow discharge nitrogen plasma treated Ti alloy can potentially be used for orthopedic applications.

3.2Background and specification

3.2.1Introduction

Integration of implants within the body is a long-standing problem in medicine and tissue engineering. Although most tissue engineering research has focused on interface formation, the tissue-implant interface generated by the host tissue should maintain

stability under physiological loading conditions[29]. The success of any implant surface modification treatment effort requires a thorough in vitro and in vivo estimation of the surface architecture-interface bonding strength relationship existing at the native insertion site of the implant [30]. Surface (e.g. roughness, porosity), mechanical (e.g. hardness, fracture strength), and biological factors (e.g. osteointegration to host bone, osteoconduction, osteoinduction, and osteogenic) are critical for the design of the surface modification technique for an implant. Application of surface modification techniques (e.g. micro to nanoscale grooving, micro to nanoscale ion coating) to improve the mechanical and biological performances of an implant in active area of research [31-34]. However only a few studies have been conducted to evaluate the effects of these treatments on the mechanical strength of the implant/biomaterial interfaces. When functional static loading exerted via the implant exceeds a certain stress limit the implant is regarded as being "overloaded", leading to possible complications such as peri-implant bone resorption [35]. For clinical practice, an implant must maintain initial fracture strength of the bond due to physiological static loading [36]. Therefore, the study of any surface modification treatment (such as plasma-surface modification techniques) effect on the fracture strength of the implant/biomaterial interface is an important factor to determine for the design of the treatment method. Plasma-surface modification techniques such as plasma spray, plasma immersion ion deposition, which are proven to be economic and effective, have already been widely applied in the modification of biomedical implants [14, 37-41]. The unique advantage of plasma modification over the other methods is the ability of selectively enhancing surface properties (within several hundred nanometers), whereas the bulk contributions remain unchanged [14]. Plasma immersion ion deposition is a versatile technique that can conduct multiple processes, such as simultaneous and consecutive implantation, deposition and etching of the implant surface. Another major advantage of the technique is the omnidirectional processing capability to tailor the surface properties of many biomaterials, including metals, ceramics and polymers, by introducing a variety of different kinds of elements and functional groups into the materials with complex shapes [37-39]. There are sophisticated

thin film deposition techniques to get nitride thin films. On the other hand, a much simpler way of attaining nitride on Ti alloy is by a simple direct current (DC) glow discharge of nitrogen plasma treatment on the alloy. However, the influence of the plasma nitride treatment on the surface, mechanical and biological properties of Ti-6Al-4V Eli are not known. This study measured surface (roughness), and mechanical (hardness, interface fracture strength of titanium/biomaterial) properties due to the application of glow discharge nitrogen plasma treatment on Ti-6Al-4V alloy.

This study considered titanium/polymethymethacrylate (PMMA) bone cement as the model for measuring the effect of plasma nitriding on the mechanical strength of titanium/biomaterial interface. Among many factors, surface characteristics (e.g. energy, roughness and hardness) of implant affect the propagation of the flaw created at the interface between implant and cement [42]. In vitro [14] and in vivo [40] surface characteristics of implant can be varied by plasma ion deposition on the implant. Micron to nanometer size architectural changes at the interface by deposition of plasma nitride on Ti alloy can improve the fracture strength of Ti/biomaterial interfaces. In this project studied the deposition of TiN on Ti-6Al-4V ELI alloy by DC glow discharge plasma nitriding treatment to improve the bond strength between the metal implant and bone cement. This study hypothesized that plasma nitriding treatment on Ti alloy may alter the surface chemical and mechanical states of the Ti alloy that may influence the fracture strength of implant/cement interfaces under static load.

3.3Material and method

3.3.1Sample Preparation

This study used titanium alloy, Ti-6Al-4V Eli (ASTM B 348 standard, grade 23, biocompatible) as the titanium implant. Among the various Ti alloys, Ti-6Al-4V Eli is used in this study because of its better physical and mechanical properties in comparison to pure Ti [8]. The Ti-6Al-4V Eli titanium alloy round bar was referred in this study as the Ti bar. Ti bar (76 mm length and 9.565 mm diameter) were purchased from Titanium

Metal Supply, Inc., Poway, CA. Ti rods of 76 mm length were used for surface roughness and pull out tension tests on the Ti-PMMA bone cement samples. Cobalt™ HV bone cement (Biomet Inc., Warsaw, IN) was used as the PMMA cement. According to manufacturer recommendations, PMMA cement was prepared by hand mixing 2.2 grams of PMMA powder with 1.1 ml of methyl methacrylate (MMA) monomer using powder: monomer ratio of 2:1. The above two sizes of Ti rods without plasma treatment was referred as control.

Both control and plasma treated Ti samples were polished before experiment using Buehler three steps polishing techniques recommended for titanium [43] as described in detail in Khandaker et al. [44]. The reasons of polishing of Ti bars were to have uniform surface morphology for all tests samples. Ti rod samples having length 76 mm were circumferential polished up to 12 mm from an edge. Briefly, the polishing steps consist of using Buehler CarbiMet 2 Abrasive paper to polish the surface for 5 minutes with 9um MetaDi Supreme Diamond Suspension spray on the contact surface of the Ti and the polishing disc. Then polish of Ti surface again was using Buehler Ultra Pad cloth with 0.05um MetaDi Supreme Diamond Suspension spray on the polishing surface for next 5 minutes. Finally the Ti surface was polished using Buehler MicroCloth and MasterPrep Alumina for 5 minutes. After each step, Ti rods were cleaned by ethanol.

3.3.2Nitrogen-plasma treatment

Tension DC glow discharge nitrogen plasma treatment on both sizes of Ti samples was conducted at Amethyst Research Inc. (Ardmore, Oklahoma, USA). This plasma system was developed for multiple materials modification applications; including hydrogen defect mitigation in semiconductors as well as surface modification and surface etching to remove contaminates. A schematic of the plasma system is shown in Figure 3-1(a). The plasma is generated by applying a positive voltage across the top plate and a negative voltage to the bottom plate. This voltage difference is typically about 370 V. In case of nitriding of Ti-rods, the samples were placed in the middle of the bottom plate. The electrode plates were placed 3 cm apart putting +185 V to top plate and -185 V to the

bottom. Research grade nitrogen gas was flown between the plates to generate nitrogen plasma, which resulted in the formation of Ti-N on the Ti surface. DC glow discharge nitrogen plasma was applied on the polished side of each kind of Ti samples for 4 hours. A picture of glow discharge plasma is shown in Figure 3-1(b).

3.3.3Surface morphology

The influence of Ni-plasma treatment to surface morphology of 76 mm length Ti samples around the circumference was evaluated by Leica DCM8 surface metrology instrument using 50x bright field confocal control condition. Scanning was conducted over 350.622 µm length × 263.934 µm width × 10.7763 µm length for both plasma and control samples. Height parameters, topography and intensity layers images were compared.

3.3.5Pull out tension tests on titanium/cement samples

A 3D printed (Dimension elite 3D printer) cylindrical holder was used to cure the cement around the plasma treated or non-treated rod ends for finding the fracture strength of each groups of Ti/cement samples. A 76 mm length Ti rods was used for the pull out tension test on a Ti/cement sample. Figure 3-2(a) shows the fabricated holder for the production of Ti/cement samples. Test Resources Universal testing machine (UTM) was used for the pull out tension tests on Ti/cement samples as shown in Figure 3-2(b). The detail of the test method for pull out tension tests on a Ti/cement sample can be found in Khandaker et al. [44]. Briefly, Ti samples with or without plasma treatment were potted in the holder using Cobalt HV PMMA bone cement. PMMA bone cement were prepared according to the manufacture protocol and poured it into the holder during the doughy phase. A plate that has a tube extruded from the center of the plate was used to press cement in to the gap (~2.8 mm) between holder and Ti rod. The plate was pressed by hand to encapsulate the bottom end of the Ti rod with cement up to 10 mm. The plate was bolted with the bottom gripper of the UTM and cement was cured for 15 minutes. A set of weights equivalent to 60 kPa on the cement was applied to the top of plate for

curing of cement for all test samples under same pressure. After cured, the pull out static test was conducted at strain rate 0.05 mm/sec. The maximum pull out force was determined from the recorded load-displacement plots from the tests. After the test, the samples were pulling out from the plastic holder. The holder was cut in to half using saw machine to accurately measure Ti-cement contact length and area. The fracture strength was calculated by dividing the force at the point of failure by the surface area of the implant in contact with the cement.

3.3.6Statistical Analysis

A one-factor analysis of variance (ANOVA) with subsampling assuming unequal variances was performed in SAS v. 9.3 using proc mixed to determine if there is a significant difference in the mean hardness and cell densities of the control and plasma treated groups. An independent samples t-test assuming unequal variances was performed to determine if there is a significant difference in the mean fracture strength of the control and plasma treated groups.

3.4Results

Though a clear difference of topography and intensity layers confocal microscope images were observed (Figure 3-3), but the roughness parameters data (Table 3-1) showed no noticeable changes of the roughness between the plasma nitride treated Ti samples and control. This result suggested no significant distortion of the surface due to the nitrogen plasma treatment. The change in roughness due to plasma treatment on the Ti surface was within ±2 nm range.

The comparison of the load-displacement plots of a control and plasma treated specimen is shown in (Figure 3-4). A sudden increment of load was observed for all specimens at the initial stage. Such high initial load was higher for plasma treated samples compared to the control samples. The figure also shows that the slope of the load vs. displacement values for all samples are steeper at the initial stage of the

experiment than at failure condition, which means a higher load are required at the initial stage than failure stage. The increment of load with displacement behaved linear until the onset of cracking which is observed in the figure by the nonlinearity (fracture initiation) point of the load-displacement curve. Also, Figure 3-4 shows that the plasma-treated specimen requires more fracture load than the control specimen. Results show that the amount of displacement before the initiation of crack at the interface is different between control and plasma treated samples. The values of fracture strength of both samples were calculated. The experimental parameters and mean fracture strengths for the control and plasma treated samples groups determined from the pull out tension tests are displayed in Figure 3-5 and Table 3-2. There is a significant difference in the mean fracture strengths of the groups ($t = -4.76$, $p = 0.016$). These results suggested that plasma treatment have a positive influence on the bonding between titanium and cement.

3.5 Discussion

The difference in fracture strength between control and nitride treated samples is mainly due to the difference in surface conditions between the plasma treated and control Ti samples. The difference in residual stresses due to plasma nitriding can be the main reason for the improvement of the fracture strength at the titanium-cement interface by plasma nitriding treatment. The localized residual stresses due to hardness and surface energy differences at the interface of Ti-cement caused by plasma nitriding treatment can be higher than control Ti-cement, which resulted in higher fracture strength for plasma treated Ti-cement compare to control. This discussion is in agreement with Kim et al. [45] who found that the molecular dissipation of the polymer in the vicinity of the interface is the major cause of the practical energy of separation of polymer/metal interfaces. According to the authors, mechanical interlocks promoted by plasma adsorption provoke energy dissipation processes during fracture, which practically constitute the adhesion strength of a metal/cement interface.

The difference of the surface roughness between plasma treated and non treated samples were found in the nanometer scale which are in agreement with Ferraz et al. [46]. This

difference in results was due to the difference in the plasma treatment conditions. According to the author's knowledge, there is no study conducted to evaluate the effect of the plasma treatment on the interface fracture strength of Ti-cement interfaces. Therefore, the author is unable to compare the interface fracture strength of plasma-nitridited Ti-cement compared with untreated Ti-cement samples. The improvement of the interface fracture strength of plasma-nitridited Ti-cement compared to untreated Ti-cement samples is reasonable since plasma treatment effect the localized residual stress on the titanium surface that positively influences the bonding between the titanium and cement [47]. In vivo studies on rabbit femurs by Ferraz et al. [48] found that plasma treated Ti implants can induce a similar bone response to the untreated ones. Since the plasma nitride treatment method developed in this study improved the physico-mechanical properties of Ti without affecting its biocompatibility, therefore, it can be concluded that Ti-6Al-4V-Eli surface modifications by DC glow discharge nitrogen plasma can favor in vivo bone formation in order to develop improved Ti alloy surface.

The originality of this study is the evaluation of a DC glow discharge nitrogen plasma treatment on titanium alloy for improving its surface properties. Specifically, this study measured the effect of plasma treatment roughness and hardness of Ti-6Al-4V Eli as well as determined on the adhesion strength of the Ti alloy with an orthopedic bone clement. This study will lead to the development of a surface modification technique for improving the biomechanical performances of Ti-6Al-4V Eli for orthopedic or orthodontic applications. The importance of the article is the utilization of nitrogen plasma used in semiconductor industry for nano-scale surface modification and defect passivation.

This study was limited to a specific amount of time, nitrogen flow rate and voltage differential between the plates that was used to generate a nitrogen plasma, which resulted in the formation of Ti-N on the surface. The effect of the thickness of TiN, which can be varied by adjusting the plasma treatment conditions, on the mechanical and biological parameters would be an interesting study, however, was not considered here. Further improvement of the fracture strength of the implant-cement interface can be

achieved by the optimization of the Ni-plasma treatment through the nitrogen discharge time, gas flow rate, and the voltage across the top plate and bottom plate in the plasma chamber. In addition, nanoparticle additives incorporated into the cement can be used which will further diminish local contact stresses at the implant-cement interface as found in our earlier study for the bone-cement interface [49].

3.6 Conclusion

The objectives of the study were the evaluation of the surface morphology, and interface fracture strength of Ti due to a nitrogen plasma treatment on Ti implant. This study concluded that the nitrogen plasma treatment influenced the hardness, and energy of conventional Ti-cement interfaces, which lead to the enhancement of the bonding of Ti alloy with bone cement compared to the untreated samples. DC glow discharge plasma nitriding treatment on Ti surface can potentially improve the union between Ti-cement interfaces.

3.7Figures

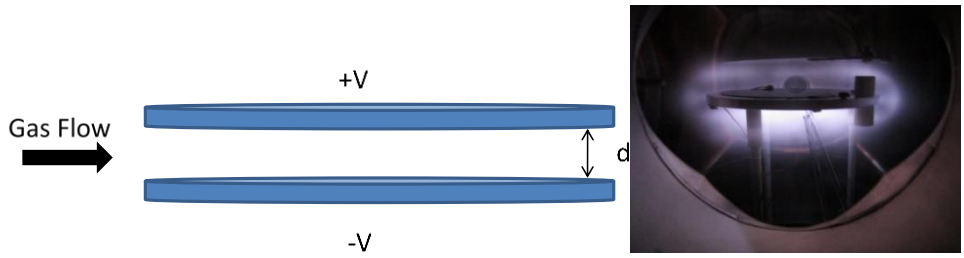

Figure 3-1 (a) Schematic of plasma setup showing the top and bottom plates separated by a distance, d and (b) Glow discharge Plasma.

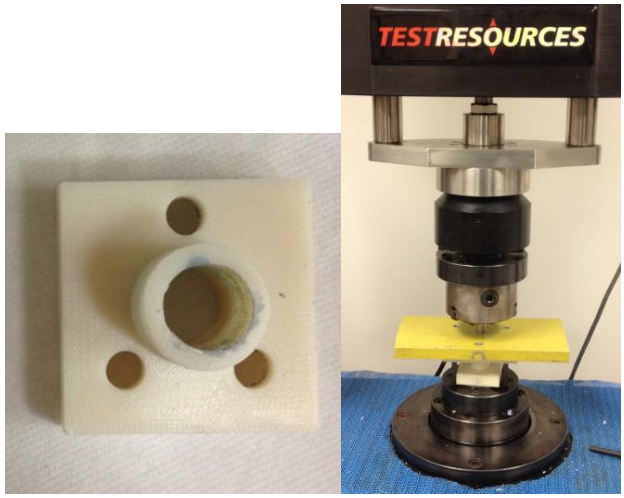

(a) (b)

Figure 3-2 (a) Fabricated holder for static test, and (b) Static tests setup on UTM

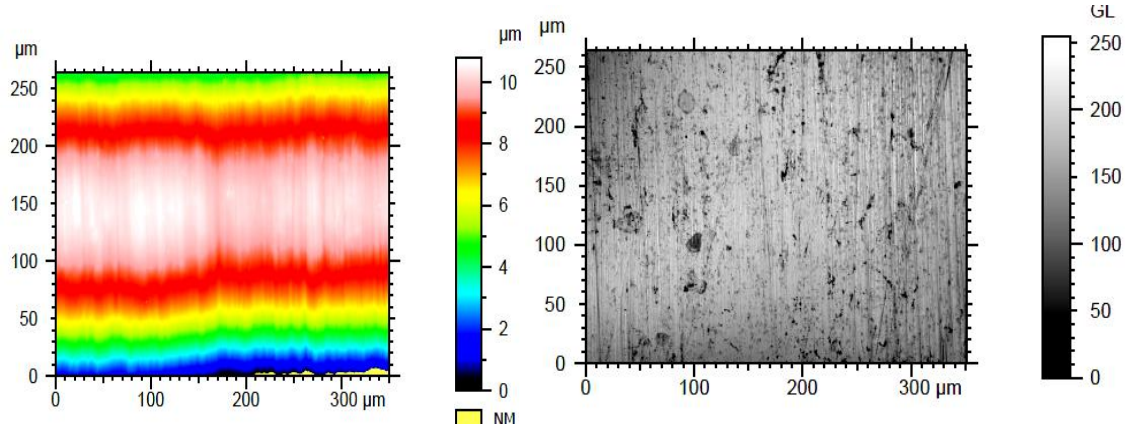

(a) (b)

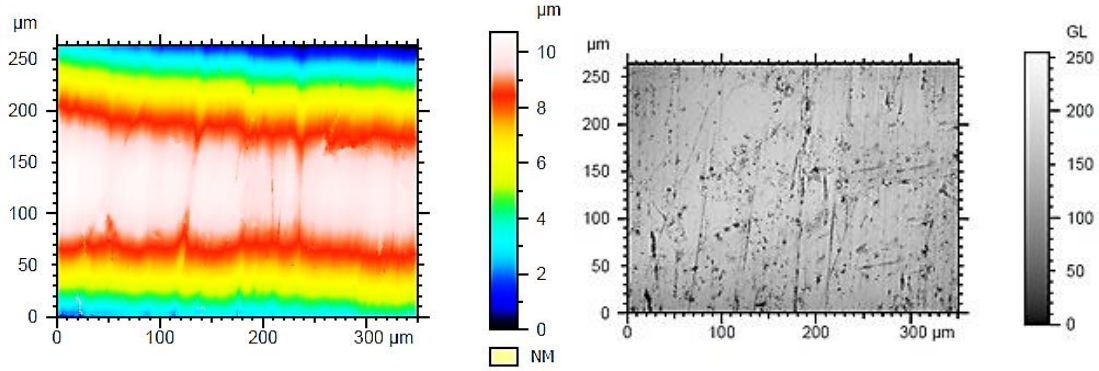

(c) (d)

Figure 3-3 (a) Topography and (b) intensity layers confocal microscope images of a Ti sample. (c) Topography and (d) intensity layers confocal microscope images of a plasma treated Ti.

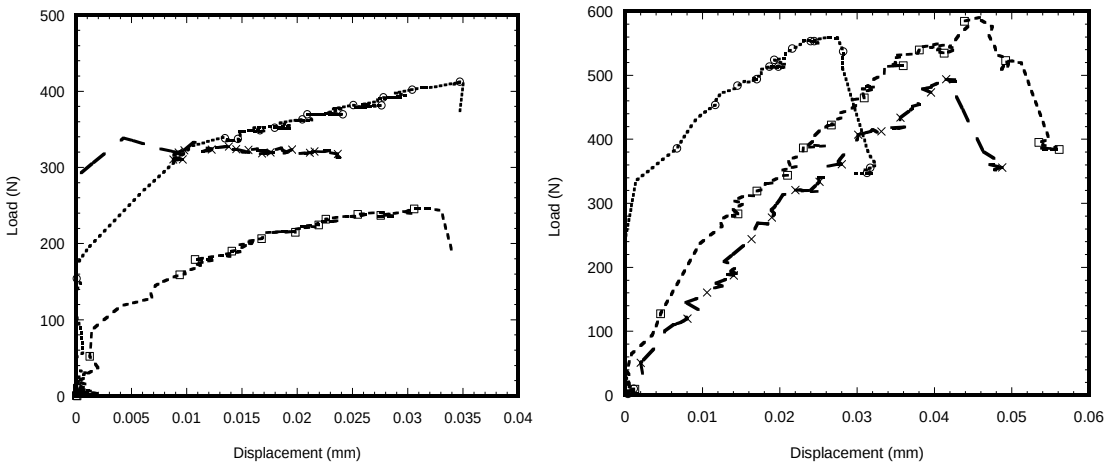

(a) (b)

Figure 3-4 Load-displacement curves of 3 samples during the static tests on Ti-cement interfaces: (a) control and (b) plasma treated samples.

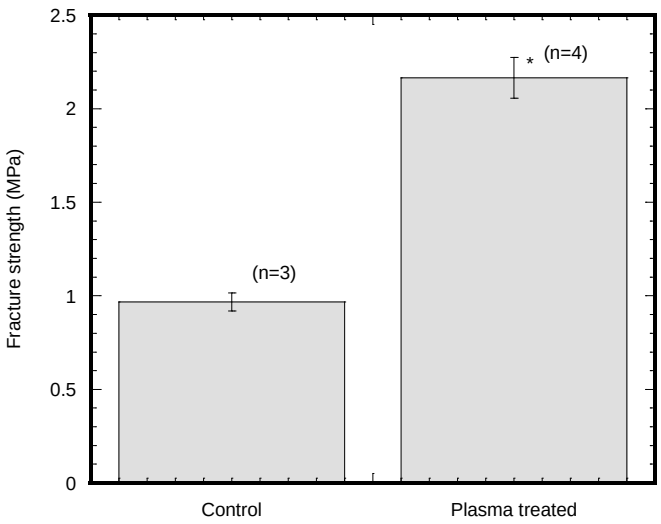

Figure 3-5 Bar diagram of the variation of fracture strength of control samples (Ti) with plasma treated samples, Data presented as means ± standard error of mean; n=3 for control; n=4 for the plasma treated samples. Note: *p<0.05 (compared to PMMA)

3.8Tables

Table 3-1 Some specific parameters of surface

Parameter Description	Control	Plasma treated
Root Mean Square Roughness (Sq)	2.50 µm	2.52 µm
Skewness (Ssk)	-0.92	--0.72
Kurtosis (Sku)	2.95	2.43
Max Peak Height (Sp)	3.12 µm	3.43 µm
Max Valley Depth (Sv)	7.65 µm	7.28 µm
Max Height of Surface (Sz)	10.77 µm	10.72 µm
Average Roughness (Sa)	2.07 µm	2.13 µm

Table 3-2 Summary statistics for static tests experimental data by group

Parameters descriptions	Control	Plasma Treated
No of samples tested	3	4
Length of implant-cement interface (mm)	10.23 ± 0.18	9.26 ± 0.18
Contact Area (mm^2)	307.34 ± 5.47	276.28 ± 5.29
Fracture load (N)	329.21 ± 41.05	600.60 ± 111.48
Fracture strength (MPa)	1.05 ± 0.14	2.16 ± 0.43

CHAPTER 4

IN VIVO EVALUATION OF THE ELECTROSPIN FIBER TRATMENT EFFECT ON TITANIUM/BONE INTERFACES

4.1 Summary

Microscale topographies can be fabricated on titanium (Ti) alloy implant using microgrooves that allow nanofiber mesh (NFM) to be deposited along the groove. The effect of depositing of collagen (CG)-poly-ε-caprolactone (PCL) NFM at the microgroove of Ti on the mechanical stability of the implant with bone was investigated in this study using a rabbit model. This study hypothesized that deposition of collagen-poly(ε-caprolactone) nanofiber mesh (CG-PCL NFM) coating at the microgroove can improve *in vivo* mechanical stability and osseointegration of Ti with bone. Three groups of Ti samples were produced: control Ti samples where there are no microgrooves or CG-PCL NFM, groove Ti samples where microgrooves were machined on the circumference of Ti, and groove-NFM Ti samples where CG-PCL NFM was deposited on the machined microgrooves. Each group of Ti samples was implanted into rabbit femurs for 8 weeks. Mechanical stability was quantified by shear strength of Ti/bone samples from a pullout tension test. This study found that the shear strength of groove-NFM Ti/bone samples were significantly higher compared to control and groove Ti/bone samples, respectively. The study concludes that orthopedic implants containing microgroove and CG-PCL NFM coating can improve *in vivo* mechanical stability of implant with bone.

4.2 Background

Titanium (Ti) alloy is the most widely used implants for orthopedic and orthodontic surgeries because of its strong mechanical, chemical and biological properties [5, 16, 50, 51]. Although considerable advances have been made in improving the biological performances of Ti alloy implants, an ideal implant for these surgeries is still not achieved. Two types of fixation methods, cemented and cementless, are commonly used

to hold an implant in place. Cemented fixation, mainly used for osteoporotic bone, requires bone cement to hold the prostheses in place [6], whereas cementless fixation, mainly used for healthy bone, relies on bone growing into the surface of the implant for fixation [52]. An ideal implant for cementless surgeries should ensure lifelong mechanical stability and induce osseointegration with the adjoining tissues [53]. If the implant surface is inadequate for osseointegration, micro-motion occurs at the implant surface leading to activation of osteoclasts' resorption of bone around the implant, contributing to further implant loosening and eventual implant failure [54, 55]. Each year in the US, 40,000 hip arthroplasties have to be revised because of painful implant loosening and it is expected that the rates of revision will increase by 137% for total hip and 601% for total knee revisions over the next 25 years as the population ages [56]. Revision surgeries are required for implant failures that are costly and painful. Because Ti implant loosening leading to joint replacement surgery usually occurs from lack of osseointegration of the implant with the bone, clinically better osseointegration of implant with bone are required for the surgeries.

The differences between natural tissue-tissue and tissue-implant interfaces are mainly due to the difference in contact geometry and material properties of the implant. Natural tissue-tissue interfaces have a mechanical interlock with naturally occurring osteogenesis between the joining tissues. However, the surface of implants without treatments do not currently provide for an adequate mechanical interlock and fail to provide osteogenesis to mimic native tissue-tissue geometry and mechanical responses. The motivation of this study is to improve titanium implant surface topography and osteogenesis activities for cementless implant surgeries that will mimic the native tissue-tissue joint.

Micron to nanometer size grooves can control the cell settlement on the implant surface or be used to direct tissue generation at the implant/bone interface [57]. Various researchers created different groove topographies on the implant surface using surface cutting/etching, and ion deposition techniques [57-60]. Such grooves facilitate the formation of extracellular matrix on the implant surface. Extracellular matrix provides the

principal means by which mechanical information is communicated between tissue and cellular levels of function [61]. These mechanical signals play a central role in controlling cell fate and establishing tissue structure and function [61]. Implant surfaces can also be improved by mimicking the natural extracellular matrix of bone tissue, which is a highly organized nano-composite [59]. Electrospinning is a process by which organized fibers with micro- to nanometer diameters can be deposited on Ti surfaces from an electrostatically-driven jet of polymer solution through a needle [62, 63]. Khandaker and Snow developed an electrospin technique (U.S. Patent Application No. 14/734147, International Patent Application No. PCT/US15/45183, and U.S. Patent 9,359,694) by which a single strand of Polycaprolactone (PCL) NFM can be deposited on a titanium (Ti) implant [64].

Electrospun PCL nanofibers shaving a high surface area-to-volume ratio, is biocompatible and nontoxic, and was used as a carrier for local drug delivery [65, 66]. Electrospun PCL NFM can be used to support the extracellular matrix protein for bone tissue generation inside the microgroove on a Ti surface. The application of the PCL electrospun fiber as an NFM coating material for Ti implants has not been investigated yet. The problem of coating PCL NFM on implants is the poor adhesion with the implant surface. Khandaker and Riahinezhad recently developed (U.S. Patent Application No. 62312041) a set of steps by which electrospun PCL NFM can coat in microgrooves on orthopedic and orthodontic implants. The effect of coating the microgrooves with NFM on the mechanical stability and osseointegration of Ti is not known and investigated in the present study.

Collagen (CG) is the major insoluble fibrous protein in the natural extracellular matrix and in connective tissue [67]. Research shows that collagen-coated biodegradable polymer nanofiber mesh has potential for both *in vitro* and *in vivo* cells growth [68, 69]. Multilayers of aligned single strands of PCL ENF can be deposited on Ti implants using an electrospin process. Surface geometry and biocompatibility determines the interaction of proteins and cells with the implant surface [70]. Controlled fabrication of

microgrooves on titanium surfaces and filling those microgrooves with CG-PCL NFM can improve the mechanical responses and biocompatibility properties of the implant. The increased mechanical interlock that can be created by microgrooves is associated with better cell adherence, higher bone-implant contact, and improved biomechanical interaction. The changes in the biocompatibility of titanium surfaces by a CG-PCL matrix network may influence cell attachment, proliferation, and protein adsorption capability to the matrix [71]. Therefore, the objective of this research is to measure the effects of grooving and CG-PCL NFM treatments on the *in vivo* mechanical stability and bone responses of Ti.

4.3 Materials and Methods

4.3.1 Materials

Ti wires (6Al-4V ELI, ASTM B 348 standard, grade 23, biocompatible) of 2.26 mm diameter and 12 mm length were purchased from Supra Alloys Inc., Camarillo, CA. PCL solution was prepared by mixing PCL pellets (pellet size~3 mm, average M_n 80,000) with acetone (laboratory reagent ≥99.5%). Both PCL and acetone were purchased from Sigma Aldrich (Sigma-Aldrich Co. LLC., St. Louis, MO). Rat tail type I collagen (Discovery Labware Inc.) was purchased from Dow Corning.

4.3.2 Specimen design

Figure 4-1 shows the steps followed to the find the in vivo mechanical strength of Ti/bone interfaces. Three groups of implants were used in this study: control, groove and groove-NFM as schematically represented in Figure 4-2. Ti implants without grooves and NFM were named control samples (Figure 4-2 (a)). Ti samples having machined microgrooves along circumferential surface were named groove samples (Figure 4-2 (b)). Ti samples having microgrooves with CG-PCL NFM were named groove-NFM samples (Figure 4-2 (c)).

4.3.3 Preparation of Ti samples

4.3.3.1 Control samples

All groups of Ti samples were polished using a drill machine check and gripper as shown in Figure 4-3. Ti wires were all polished in order to have uniform surface morphology for all test samples. Ti wires samples were circumferentially polished up to 8 mm from one end. The three steps polishing technique, as recommended by Buehler [72], was used to polish the Ti surface. The first step was to polish the surface using Buehler CarbiMet 2 Abrasive paper with 9µm MetaDi supreme diamond suspension spray on Ti. The second step was to polish the Ti surface again using a Buehler Ultra Pad cloth with 0.05µm MetaDi Supreme Diamond Suspension spray. The third step was to polish the Ti surface using Buehler MicroCloth with MasterPrep Alumina polishing suspension. Each polishing step was conducted for 2 minutes. Ti wires were cleaned by ethanol after each step and finally autoclaved at 121°C. Ti wires without further treatment were considered as control samples.

4.3.3.2 Groove samples

A diamond saw blade (Buehler Isomet wafer blade 76.20 mm diameter ×0.15mm thickness, 15HC) was used to machine the microgroove on the circumferential surface of the wire (Figure 4-4). Ti wire was fastened with the shaft of a motor. The motor was secured in the saw machine at the sample grip holder. Each microgroove was created by running the motor and saw machine simultaneously in opposite directions for 8 seconds. Eighteen bands of circumferential parallel grooves were created starting at a 0.5 mm distance from one end of the Ti wire. The microgrooves are 0.05 mm apart from each other. All samples were cleaned in an ultrasonic cleaner followed by 70%ethanol and then autoclaved at 121°C. Ti wires with only microgrooves were classified as groove samples.

4.3.3.3 Groove-NFM samples

Ti samples having grooves were exposed to plasma O_2 for 5 minutes in a Zepto low pressure reactive ion etching system (Frequency: 40 kHz, power 30 watt) to increase the attachment of collagen to the Ti surface. Ti wire was soaked with a collagen solution and PCL electrospun nanofiber was deposited on the Ti. Aligned PCL nanofibers were deposited on the grooved Ti samples using an electrospin setup (Figure 4-5). The details of fabrication of PCL electrospun nanofiber can be found in Khandaker *et al* [73]. In short, PCL pellets (7.69 wt%) were mixed with acetone in an ultrasonic (Sonics & Materials, Inc., model # Vibra-cell VCX 130) mixer. The sonication process was carried out at approximately 60°C for 30 minutes. The solution was poured into a glass syringe on an infusion pump (Harvard Apparatus, mode # PHD ULTRA) for PCL fiber production. PCL melt was ejected from the glass syringe through an electrically charged needle (23G blunt needle, 1 in length, model # BX 25). The needle was charged by a high voltage power source (Gamma High Voltage Research, Inc., model # ES 30 series). Aligned PCL fibers were collected between two parallel wires. The topography of fibers on carbon tape was analyzed using a scanning electron microscope (Hitachi TM 3000).

Collagen solution was prepared by mixing 2.3 microliters of type I collagen with 0.23 microliters of acetic acid (0.02 M) and 195 microliters of deionized water in a vortex mixer. Ti wire was soaked with the collagen solution. Aligned PCL ENF were deposited on the Ti by manually rotating the Ti wire 6 times and dried in UV chamber. Finally, CG solution coating on Ti were applied again and dried to prepare the groove-NFM Ti samples. The groove-NFM samples were kept at 4 degrees C until implantation in the rabbit femur.

4.4 Animal surgery

Each group of Ti samples was implanted immediately proximal to the lateral femoral condyle of 4-6 week-old New Zealand White Rabbits (NWR) at OUHSC according to the approved IACUC protocol. A total of 18 NWR were used for this study. Rabbits were

anesthetized with ketamine and xylazine by intramuscular injection and transported to the surgical preparation room. Rabbits were given buprenorphine and oxytetracycline, subcutaneously and tattooed on an inner ear. The entire circumference of both rear legs proximal and distal to the distal femur of the rabbits was shaved, then the leg prepped with chlorhexidine scrub alternating with alcohol. The rabbits were then moved to the operating room. After a lidocaine drip to the back of the mouth, rabbits were intubated with a 3mm ID endotracheal (ET) tube. Isoflurane was administered with oxygen via the ET tube. A final surgical prep was then performed. 0.5 ml of 0.5% lidocaine was injected subcutaneously at the incision site. Surgery started once the rabbit was completely at a surgical plane of anesthesia.

A 2.5 cm curvilinear midlateral skin incision was made starting at the distal end of the body of the femur and extending distally to just below the level of the patella. The fascia latawas then excised in line with the skin incision. The vastus lateralis muscle was then retracted cranio-medially to expose the lateral condyle and the joint capsule opened sharply. A 1.96 mm diameter drill bit was used to drill a 6~8 mm depth hole perpendicularly into the lateral condyle by manual hand drill press and then Ti wire sample hand-pushed into the hole. The joint capsule, muscle layers, and subcutaneous tissue were then sutured with 4-0 vicryl in a continuous pattern and the skin closed with subcuticular pattern. X-ray images of the implantation sites were conducted immediately after surgery to measure the depth of implant inside the bone (Figure 4-6 (a)). All rabbits received buprenorphine post-operatively for 3 days and were closely monitored for food and water intake, fecal output, and healing properties.

Rabbits were euthanized 8 weeks after surgery. Soft tissues were carefully dissected off the bone (Figure 4-6 (b)). The Buehler saw machine (Figure 4-6(c)) was used to trim the Ti-bone samples to adequate size for mechanical and histological experiments (Figure 4-6 (d)). The samples were kept moist during the preparation by soaking with saline.

4.4.1 Pull out tension tests

A custom-made fixture was used to permit coaxial alignment of the implant in the direction of pull-out force. The implant was carefully fastened to the top gripper in the mechanical tester (Figure 4-7(a)) and slowly lowered to embed the sample in a low-viscosity acrylic bone cement (BioMedtrix veterinarian bone cement) (Figure 4-7(b)). Pull out tension tests were conducted on each sample at room temperature with a steady speed of 0.3 mm/min [74]until the breakage of the implant from the bone (Figure 4-7(c)). The maximum pull-out force from load-displacement curve was measured and mechanical stability (quantified by maximum shear strength) was calculated from the ratio of the force at the point of breakage of the implant from the bone and the surface area of Ti in contact with bone.

4.4.2 Statistical Analysis

A one-factor analysis of variance (ANOVA) with subsampling assuming unequal variances was performed using the statistical tools of KaleidaGraph software to determine if there was a significant effect of application of microgroove and NFM on the mechanical stability of Ti. For all statistical tests, p *value*< 0.05 was considered as the statistical significant comparison.

4.5 Results

4.5.1 Nanofiber characteristics

Figure 4-8 shows the fabricated single layer of uni-direction nanofiber between two parallel wires using our fabricated electrospin setup. It was clear from the SEM images (Figure 4-9 (a)) of the produced fiber that the fiber distribution was mainly unidirectional, although overlapping of the fibers along the direction were observed in several places too. The fiber coating thickness on the carbon tape was found to be in the range from 386 to 518 nanometers (Figure 4-9 (b)). The distance between two fibers was measured from 13.8 µm to 26.3 µm. Because the fibers were collected on the carbon tape and Ti wires in

a similar fashion, the diameter of PCL fibers on Ti wires were predicted to be in the micron to nanometer ranges.

4.5.2 Ti sample characteristics

Figure 4-10 (a-c) shows a sample from each group of test samples. Tables

Table 4-1 shows the geometric parameters of the fabricated Ti samples. Clear topographical difference among the samples was observed. From the histological analysis report, the average groove depth for 18 grooves of a groove Ti sample was found to be 75 µm, whereas the average groove depth for the same number of grooves at the groove-NFM Ti sample was found to be 71 µm. The existence of the fiber at the groove was clearly visible in groove-NFM Ti samples (Figure 4-10(c)).

Fabrication of controlled grooves by micromachining on a Ti surface and coating the grooves by multilayers of collagen PCL NFM was successfully conducted in this study. The produced CG-PCL NFM was adequately attached with Ti for *in vivo* implantation. Since NFM coating made with PCL electrospun nanofiber and collagen resided inside the groove, NFM would not take the physiological load. Therefore, the NFM remained on the microgrooves. Our *in vitro* biocompatibility tests on CG-PCL NFM coated Ti surface (not a scope of work for this article) confirmed the attachment of coating materials after 3 weeks of cell culture on Ti surface as shown in Figure 4-11(a). During the cell culture period, the coating material had to withstand the regular cell culture medium application and suction forces every 3 to 5 days. The details of our cell culture protocols for the biocompatibility tests can be found in Khandaker *et al*. [44]. It is important to note that the CG-PCL NFM coating on the Ti plate for cell viability tests were exactly same as the coating of CG-PCL NFM on the Ti wire used in the study for *in vivo* tests. In addition, post pull out observation of groove-NFM samples revealed the presence of fibers (a very negligible amount) at the Ti/bone interface as shown in Figure 4-11(b). It is important to mention that the observation was made after 8 weeks of *in vivo* implantation of the Ti sample and the sample was cleaned with water before imaging. Therefore, it can be

concluded that the CG-PCL NFM biocoating technique developed in the study created adequate adhesion with Ti at the groove to withstand the physiological loading conditions.

4.5.3 General observations of animals

All rabbits in this study remained in good health and did not show any recovery complications after surgery. There were insignificant formation of callus ossification and extraosseous material revealed after cleaning the soft tissue from the bone. At retrieval, no visual signs of inflammatory or adverse tissue reactions were observed.

4.5.4 Mechanical testing

Figure 4-12 shows a clear difference of load-displacement responses between the control and grooved samples. The load-displacement responses of groove and groove-NFM Ti samples were characterized as elastic responses and then sudden failure of the specimen with noticeable plastic region, whereas no noticeable plastic region was observed for control Ti samples. This meant deformation of bone adjacent to implant occurred for groove and groove-NFM Ti samples. Such deformation was found to be higher for groove with NFM samples compared to other samples. Figure 4-12 also showed a clear difference of maximum fracture load between NFM coated Ti samples and noncoated specimens. Figure 4-13 depicted the differences of maximum shear strength among the sample groups. Tables

Table 4-1 presents the differences of maximum shear strength with respect to diameter, average groove depth length and the length of implant in contact with bone among the Ti sample groups. The results show that the mean values of shear strength were 3 times higher for grooved Ti samples (0.837±0.672 MPa, n = 6) compared to control samples, (0.264±0.205 MPa, n=6), although the difference was not statistically

significant (*P value*>0.05). When comparing fracture strength results of grooved Ti samples coated with CG-PCL NFM, we have noticed that the ultimate shear strength of NFM coated grooved samples (4.793±0.863 MPa, n = 6) were higher (more than 18 times)compared to control samples (*P value* <0.05). No statistically significant differences of diameters among the sample group were observed (*P value*> 0.05). Also there was no statistically significant difference of the length of implant in contact with bone among the sample group (*P value*> 0.05). Therefore, the surface coating of Ti samples by CG-PCL NFM had a significant effect on the shear strength of the samples. Post-test visual inspection of the specimens revealed that failure typically occurred at the bone-implant interfaces.

4.6 Conclusion

This study established a proof of concept of microgrooving on Ti and CG-PCL coating of the grooves for improving the mechanical stability and osseointegration of an orthopedic implant. This study shows that the combined application of microgroove and extracellular matrix structure enhanced the mechanical interlock and osseointegration of an implant with the host tissue. The fabrication of surface microgrooves on Ti and local delivery of extracellular matrix protein (collagen) at the microgrooves sites allowed the increase of the mechanical interlock and biocompatibility of a Ti implant. The histologic examination confirmed that our novel technique of CG-PCL NFM coating on Ti can improve the osseointegration of Ti under load-bearing conditions *in vivo*. Moreover, the present study showed that the increase in peri-implant new bone volume is increased due to NFM coating. Therefore, implant surface modification by groove-associated bio coating can potentially improve orthopedic implants mechanical and biological responses with surrounding biomaterials. Orthopedic implants that can deliver vitamins, proteins, and minerals may then represent an interesting approach for healthy and osteoporotic patients in need of a total joint replacement.

4.7 Figures

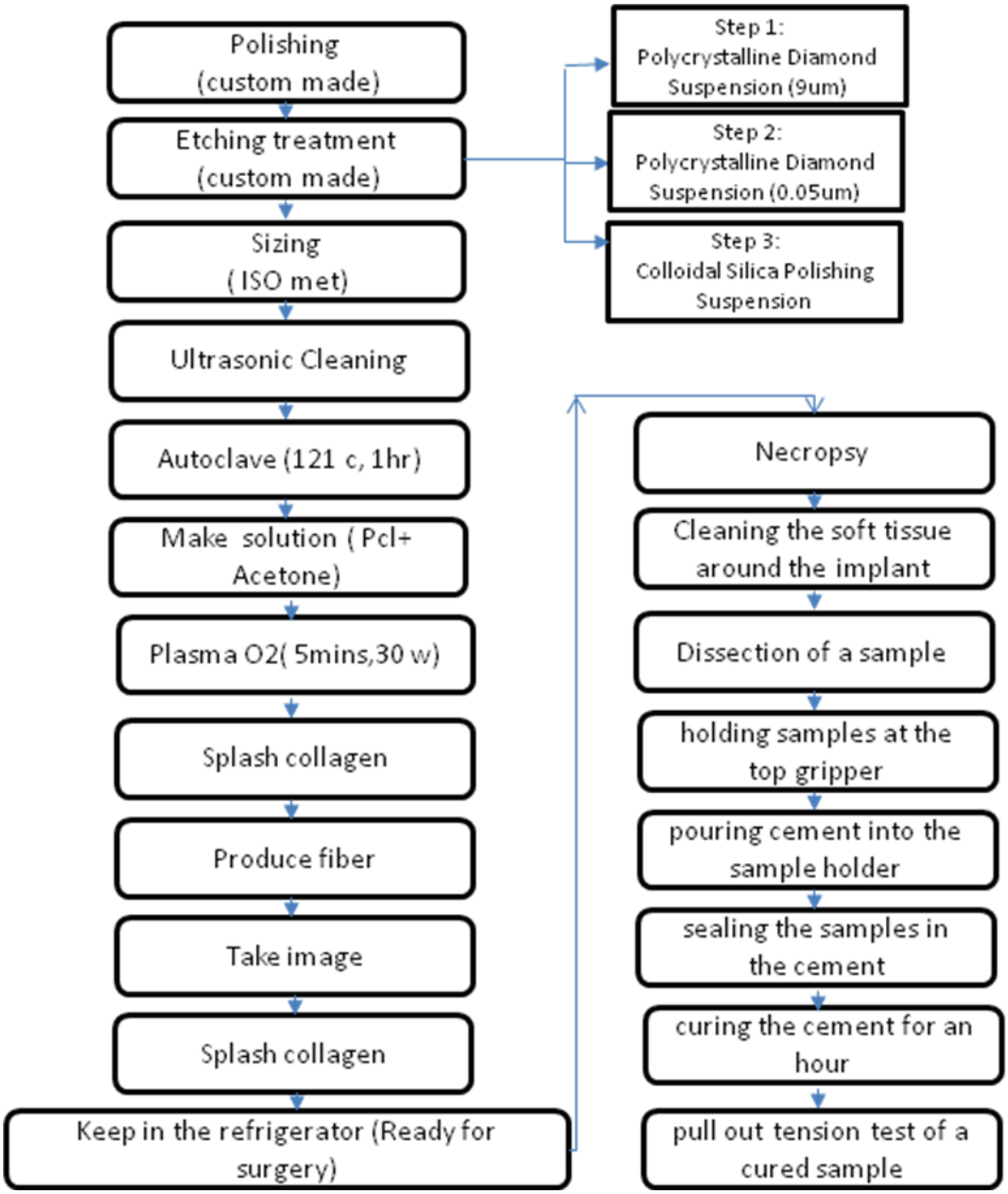

Figure 4-1. Flow chart showing the steps of determining fracture strength of Ti samples.

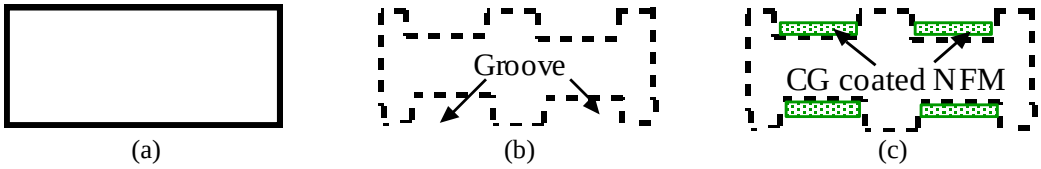

Figure 4-2. Schematic representation of longitudinal section images of a (a) control, (b) groove, and (c) groove-NFM samples

Figure 4-3. Polishing of Ti wire using a drill machine chuck and gripper

Figure 4-4. Micron depth grooving on the circumference of a Ti wire using Buehler diamond saw blade check and gripper. The gripper is holding a motor in which the shaft of the motor is secured with the implant.

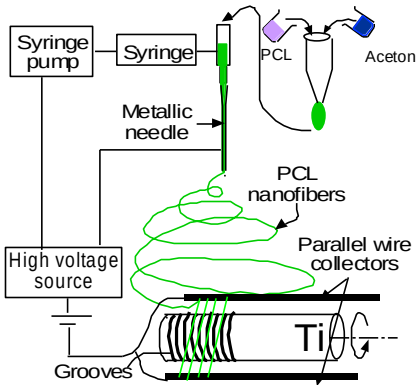

Figure 4-5.Schematic representation of coating groove Ti samples by aligned electrospun nanofiber using an electrospin process.

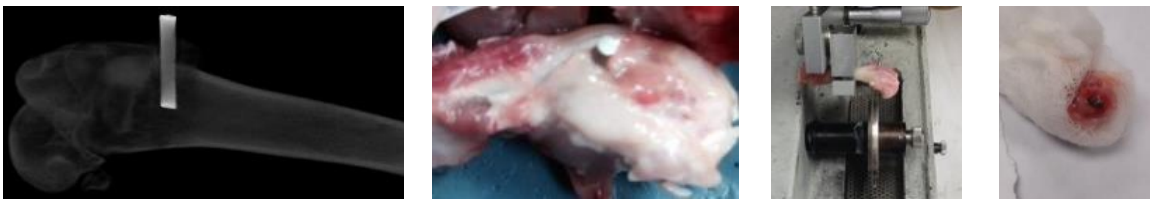

(a) (b) (c) (d)

Figure 4-6. (a) X-ray image of femur after surgery, (b) a test sample after cleaning the soft tissue around the implant after euthanasia, (c) dissection of a sample using the Buehler saw machine, (d) a sample for mechanical and histological tests after trimming.

(a) (b) (c)

Figure 4-7. Mechanical tests steps:(a) holding samples at the top gripper and pouring cement into the sample holder, (b) sealing the samples in the cement and curing the cement for an hour, and (c) quasi-static pull out tension test of a cured sample. Figure shows a sample after breakage.

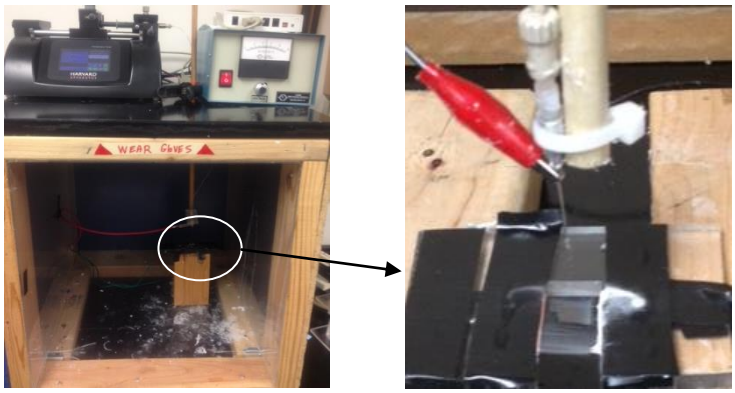

Figure 4-8. Fabricated uni-direction nanofiber between two parallel wires

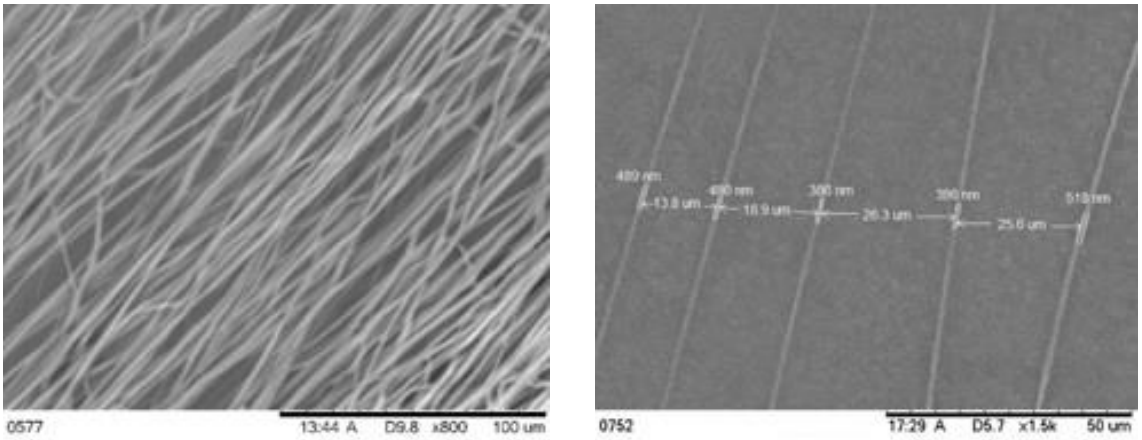

(a) (b)

Figure 4-9**.** Scanning microscope image of the aligned PCL nanofiber on a carbon type at (a) 800 X and (b) 1500 X magnifications. Figure (b) shows the diameter of the fiber and the distance between the fibers.

(a) (b) (c)

Figure 4-10. A fabricated (a) control, (b) groove, and (c) groove-NFM samples.

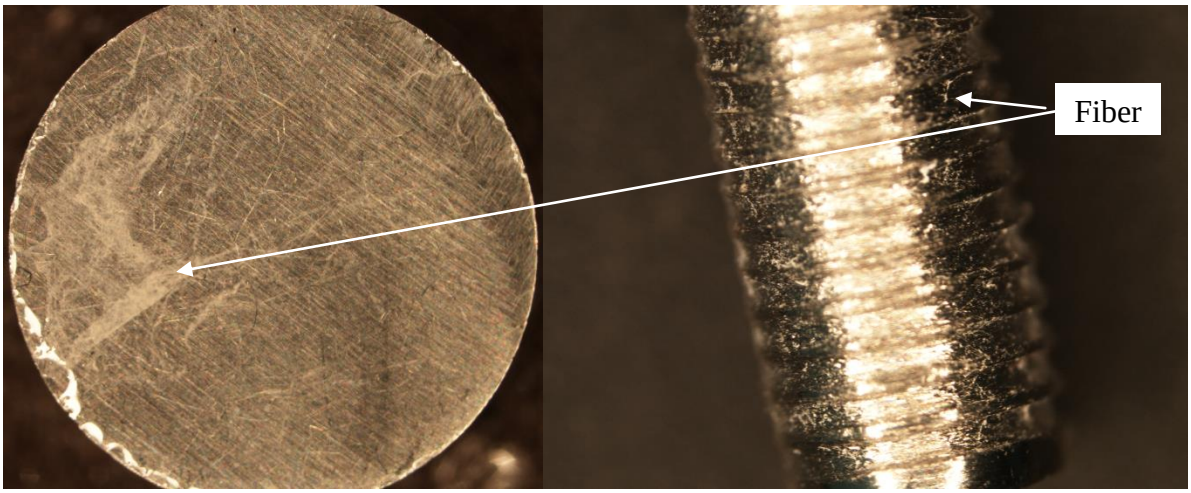

(a) (b)

Figure 4-11. (a) Attachment of CG-PCL NFM coating after *in vitro* cell culture on Ti plate after 3 weeks of cell culture, and (b) Attachment of CG-PCL NFM coating after *in vivo* implantation of Ti wire after 8 weeks.

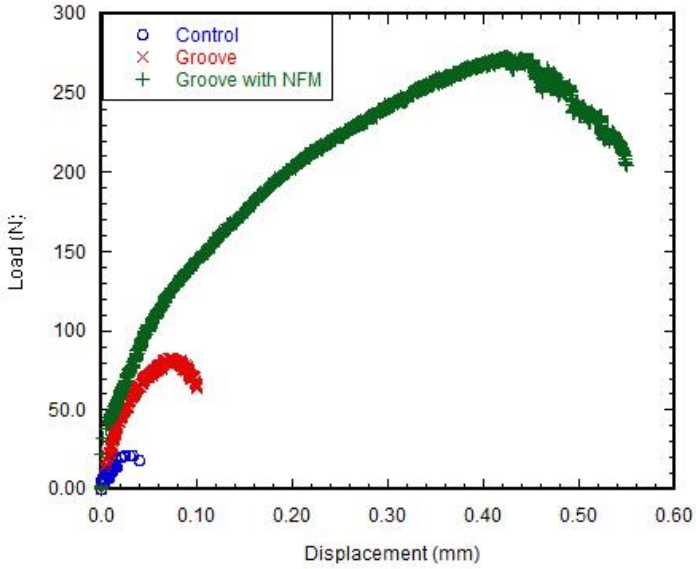

Figure 4-12. Load vs displacement plot of a control, groove, and groove with NFM samples.

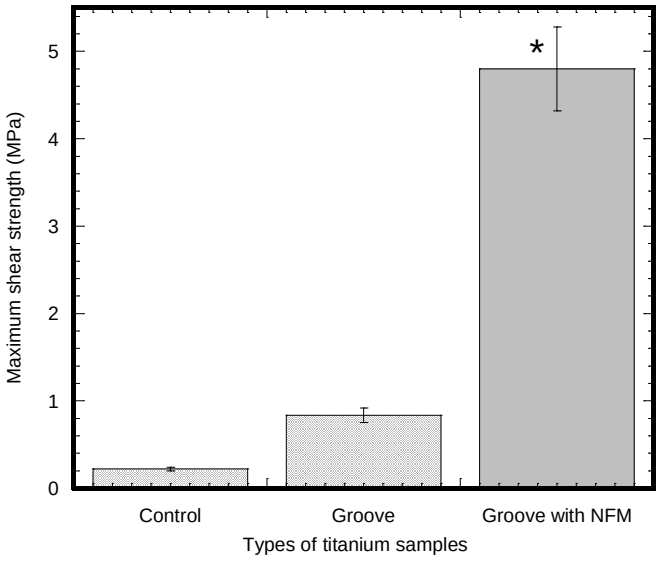

Figure 4-13. Push-out test results (in MPa) of different titanium samples after 8 weeks of implantation. Bars represent means ± SD (n = 6). * represents statistical significant results compared to control samples for *p value* = 0.05.

4.8 Tables

Table 4-1. Geometric parameters of Ti samples. The values are given as means ± =SEM (n = 6 each). * Significantly greater than control (P <0.05); †significantly greater than groove.

Sample type	**Diameter of implant (mm)**	**Average Groove Depth (µm)**	**Length of implant in contact with bone (mm)**	**Ultimate shear strength between titanium and bone (MPa)**
Control	2.203 ± 0.005	N.A.	6.628 ± 0.714	0.264 ± 0.205
Groove	2.167 ± 0.038	75.44 ± 13.72	5.680 ± 0.456	0.837 ± 0.672*
Groove with NFM	2.187 ± 0.023	71.44 ± 4.59	5.573 ± 0.224	4.793 ± 0.863*†

CHAPTER 5

IN VIVO EVALUATION OF THE MGO NANOPARTICLES EFFECT ON TITANIUM/CEMENT INTERFACES

5.1 Summary

The purpose of preliminary studies were to determine the *in vivo* effect of MgO nanoparticle on the mechanical stability of PMMA bone cemented Ti and to observe their effects on osseointegration of cement with bone using microCT scan image.

5.2 Background and Significance

The debonding of the polyMethylMethAcrylate (PMMA) cement from bone in cemented joint replacement is frequently reported in literature [75-82]. In the case of total cemented joint replacements, implant loosening occurs due to debonding of the bone-cement interface due to poor osseointegration of bone cement with bone or weakening of bone due to stress shielding [76, 78]. Current trend of biomaterial research is focused on the use of nanomedicine to solve the debonding problem by improving the osseointegration of cements with bone [54, 83-86]. The suitability of a novel cementing technique to solve the debonding problem requires complete understanding of the mechanical stability and osseointegration of cemented implant with bone. Khandaker et al. previous research reported the improvement of mechanical and biological performances of PMMA cement [87] and *in vitro* mechanical stability of bone/PMMA interface due to the addition of MgO nanoparticles with PMMA [49]. Combined applications of MgO nanoparticles and PCL nanofiber application on PMMA can further enhance mechanical stability and osseointegration of PMMA cement with bone due to enhance bioactivity and roughness of the cement surface. Such combined applications of nanoparticle and nanofiber on the mechanical stability and osseointegration of cemented implant is unknown, but can solve the debonding problem of cemented implant. The goal

of the study is to determine the effect of MgO nanoparticle on the mechanical stability of PMMA cemented Ti implant.

This project will advance orthopedic cement research by providing the understanding of how the mechanical stability and osseointegration of cemented implant can be improved by surface modification and cellular adhesion of cement by nanoparticles and nanofibers. The novelty of this project is the *in vivo* estimations of the effect of MgO nanoparticles on PMMA cemented implant. The results of the research activities will not only be applied to the improvement of cement-to-bone interface, but can also be applied to many engineering fields, such as ceramic-metal bonds and substrate -thin film coatings.

5.3 Material and Method

A total of 6 NWR animals were used to test the MgO nanoparticle effect on PMMA to the mechanical stability of PMMA cemented Ti/bone samples. Ti wires (2.2 mm diameter×12 mm length) were implanted in NWR without and with MgO nanoparticle included PMMA for the cemented Ti implant. A 2.96 mm diameter and 6 mm deep hole was made by a hand drill using the similar method used for cementless surgeries. Subsequently, the Ti wire was hand pressed into the prepared holes on both femurs of the rabbits without and with MgO nanoparticle included PMMA cement. Animal surgery and mechanical tests were conducted on the samples using the method as presented in Chapter 4.

5.4 Results and discussion

Heterogeneous application of PMMA cement around Ti was observed from the CT scan image (Figure 5-1). This is due to the difference of porosity of trabecular bone along implant. Static tension tests on cemented samples found that Ti/PMMA samples having MgO particle with PMMA (562.9 ± 166.5 kPa) has higher fracture strength compare to only PMMA cemented Ti/Bone samples (360.8 ± 291.7 kPa), although the difference between the samples was not significant (Figure 5-2). The large scatterness of

the fracture strength data was due to the heterogeneous application of cement around bone. An electrospun fiber cloth application is currently undergoing to make homogenous application of cement around Ti.

5.5 Conclusions

This research concluded that MgO nanoparticle has positive influence on the mechanical stability of the Ti/PMMA interfaces. Therefore, MgO nanoparticle has potential to be used with PMMA cement for cemented implant surgeries.

5.6 Figures

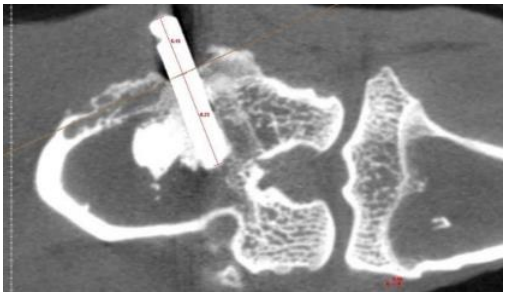

Figure 5-1 CT scan image of cemented implant

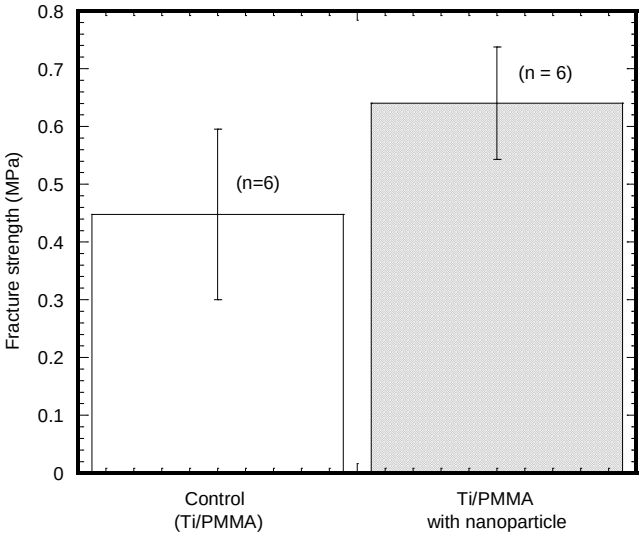

Figure 5-2 Comparison of fracture strength between with and without MgO added cemented samples.

CHAPTER 6

DESIGN AND EVALUATION OF A COMPOSITE HYDROGEL SCAFFOLD AS A BONE GRAFT

6.1 Summary

The objective of the study is to create a new 3D scaffold fabrication technique based on electrospun nanofiber (ENF) membrane and photosensitive biomedical polymer that can be used not only for *in vitro* 3D cell culture medium, but can be extended to general artificial graft for damaged soft and hard tissue. The developed composite scaffold topographical and mechanical strength was measured and compared with PEGDA based scaffold

6.2 Specification and Background

There are numerous commercially available 3D scaffold products, however none of them fulfill all the requirements for bone grafting materials. This is the reason for the constantly growing interest in the bone grafting research topic. According to literatures, current bone substitutes designed for filling bone voids caused by diseases and injuries, lack the microstructure required for successful bone growth in 3D [57, 88, 89].

Polyethylene Glycol Diacrylate (PEGDA) tissue scaffolds having thickness higher than 1 mm were shown to have limited applications as a three-dimensional cell culture device due to the inability of cells to survive within the scaffolds [90]. Without access to adequate nutrients, cells placed deep within the PEGDA tissue construct having thickness higher than 1 mm die out, leading to nonuniform tissue regeneration. PEGDA scaffold need to be designed with intricate architecture, porosity, pore size and shape, and interconnectivity in order to provide the required structural strength, transport nutrients and the micro-environment for cell and tissue in-growth. ENF membrane can be added in PEGDA membrane to intricate architecture and interconnectivity between two PEGDA

membrane layers. In additions, ENF membrane can be carrier of protein and minerals. By incorporating ENF membrane with PEGDA the biological activities (such as cell viability, degradation, and tissue generation) of PEGDA structure can not only be improved, but also the physical and mechanical properties (such as porosity, mechanical strength, ductility and permeability) can be improved. The relationship between the architecture and mechanical properties of composite scaffold is not understood yet. Knowledge of the mechanical properties of the composite scaffold with respect to fiber size, fiber organization, and ENF-hydrogel membrane composition is necessary to design and effective use of the composite scaffold for tissue engineering applications such as bone repair, which was studied in the project.

6.3 Material and Method

The process for creating a composite scaffold made with 4 layers of PCL ENF membrane and 3 layers of PEGDA hydrogel is schematically represented in (Figure 6-1). Composite scaffold was fabricated using a manual operated electrospun setup (Figure 4-8) and UV photo-polymerization (Figure 6-2) units housed in the lab. Using an electrospin setup, parallel fibers are collected between two parallel collectors. To collect multiple layers of fiber, an acrylic hollow cylindrical substrate is used to touch the aligned fiber stream, then lower it and rotate the substrate 90° and repeat the process to collect another layer. Photo-polymerization system is comprised of three major parts: 1) a UV light source, 2) mold and 3) a polymer solution. The role of the mold is to allow the PEGDA to polymerize in the desired shape. A silicone mold hollow cylindrical mold (thickness = 0.5 mm and inside diameter = 10 mm) were used to cure hydrogel according to the required shape of the composite hydrogel. PEGDA was manually injected in the mold on top of PCL ENF membrane to build the composite scaffold. A UV light source is exposed to the solution to completely cure of the PEGDA solution to solid. The thickness of the PEGDA layer of the scaffold produced in our laboratory experiments was 0.5 mm. The forgoing ENF membrane and PEGDA curing steps were repeated 3 times to make 1.5 mm thick cylindrical composite scaffold (Figure 6-3).

We have compared the SEM images of the PEGDA (Figure 6-4(a)) and PCL-PEGDA composite (Figure 6-4(b)) scaffolds. Both samples have same dimension (10 mm diameter and 1.5 mm thickness). We have compared the compressive stiffness of the PEGDA (Figure 6-4(a)) and PCL-PEGDA composite (Figure 6-4(b)) scaffolds. They were mounted between the holders in Evex mechanical test equipment (Figure 6-5). The samples were loaded up to 35 N. The load and the corresponding displacement of the scaffolds were directly recorded from Evex machine software (Figure 6-6). The slopes of the curves were used to compare the difference of stiffness between the samples.

6.4 Results

We have found that 4 layers of bi-directional ENF membranes are adequate to hold the PEGDA hydrogel liquid solution on top of PCL ENF membrane. The collection of fiber was made manually, for which a 90° rotation is almost impossible to be achieved. In addition, the ENF membrane thickness and architectures for 4 layers in composite scaffold were not same since it is impossible to collect the same ENF architecture from the manual harvesting of aligned uni-direction ENFs using the parallel wires. Similarly, the hydrogel membrane thickness and architectures for 3 layers in composite scaffold were not same, since it is impossible to deposit the same amount of hydrogel and cure under same conduction using our current PEGDA curing systems. Both this limitation will be overcome in the proposed automated system where ENF and hydrogel membrane structure will be made using a robotic arm mechanism and full atomized UV photo-polymerization systems

The test results showed that the higher surface artifacts of PCL-PEGDA composite scaffold (Figure 6-4(d)) in compare to PEGDA scaffold (Figure 6-4(c)). The stiffness of PCL-PEGDA composite scaffold (36.58 N/mm) is approximately 2 times higher in compare to PEGDA scaffold (18.64 N/mm). The results indicate that PCL-PEGDA composite scaffold strength should be higher compare to of this study confirms that PCL ENF membrane reinforced the PEGDA scaffold. Further improvement of

stiffness and other mechanical properties of PEGDA scaffold is possible by control deposition of PCL ENF membrane in the scaffold.

6.5 Conclusions

We have successfully fabricated 10 mm diameter and 1.5 mm thickness composite hydrogel. The invented composite scaffold fulfills good mechanical strength and superior microstructure requirements for tissue substitutes.

6.6 Figures

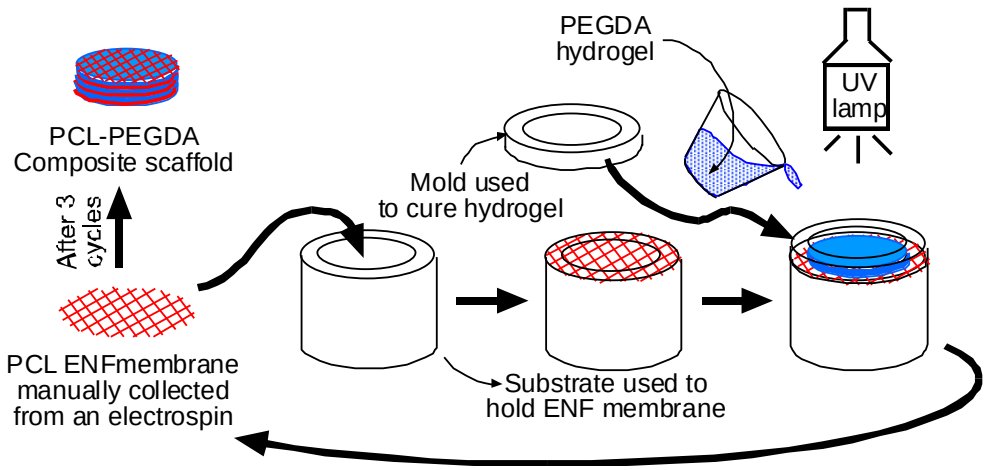

Figure 6-1 Schematic representation of the process for creating a composite scaffold made with 4 layers of PCL ENF membrane and 3 layers of PEGDA hydrogel

Figure 6-2 UV photo polymerization unit used for curing PEGDA hydrogel

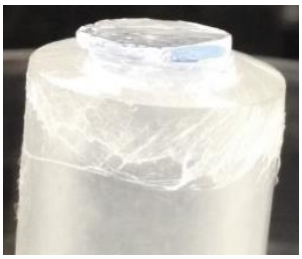

Figure 6-3 Fabricated 10 mm diameter and 1.5 mm thickness composite hydrogel on the mold.

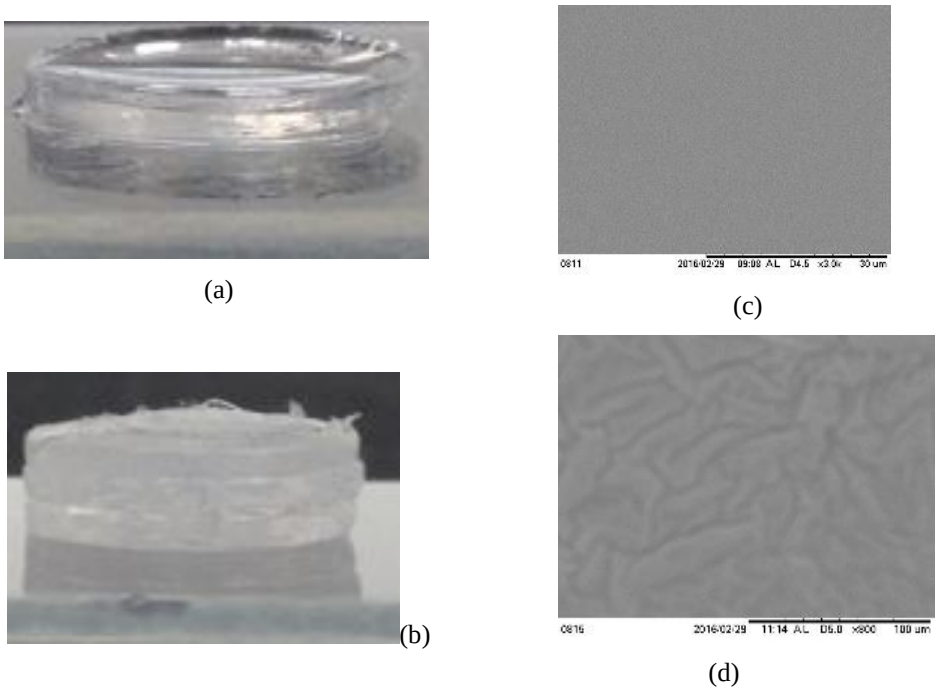

Figure 6-4 Separated composite scaffolds from the mold:(a) PEGDA and (b) PCL-PEGDA. Topographical images of composite scaffolds using SEM: (c) PEGDA and (d) PCL-PEGDA

Figure 6-5 Evex mechanical test setup for compression tests on scaffold

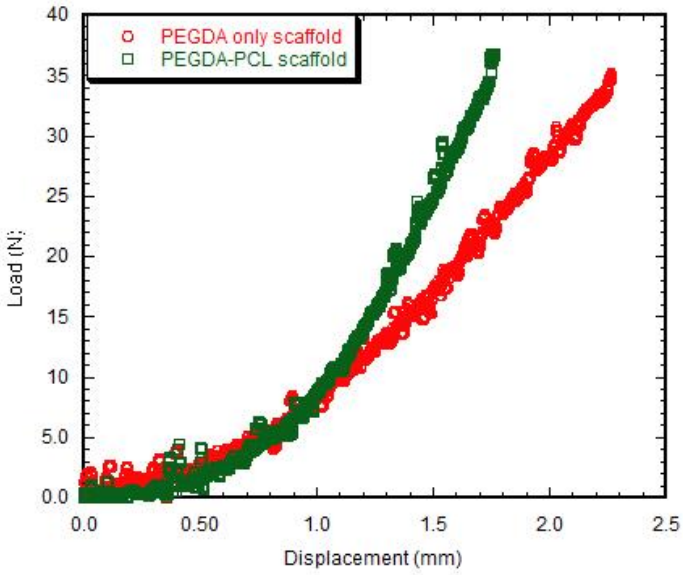

Figure 6-6 Load vs. displacement curves for scaffolds

CHAPTER 7

DESIGN AND EVALUATION OF ELECTROSPIN FIBER ANCHORED INTERVERTEBRAL DISC IMPLANT

7.1 Summary

We have studied the effect of electrospun fiber mesh anchorage on the biomechanical functions of a swelled and unswelled NP tissue EIVD models. Mechanical (compressive and viscoelastic) of the EIVD was measured using standard experimental techniques and compared with the native tissue properties. The objective was to produce EIVD which is made of silicone gel, PEGDA, and PEGDA-PCL anchored all sides by electrospun fiber. The NP and AF geometric size of designed EIVD will mimic the size of NP and AF of a rabbit tail disc. Ex vivo mechanical tests were conducted to the compare the mechanical stability between intact and EIVD implanted using rabbit tail model.

7.2 Specification and Background

Millions of people suffer from lower back pain1. Intervertebral disc (IVD) degeneration has been implicated in the etiology of low back pain. IVD degeneration is caused by the increase of stiffness in nucleus pulposus (NP), bulging of annulus fibrosus (AF) and wearing of end plate (EP) caused by the mechanical overstress to these IVD components (shown in Figure 7-1). Discectomy, spinal fusion, and total disc replacement are some of the current surgical treatments to repair degenerated discs. Discectomy and spinal fusion are complex, costly, and unable to restore the normal biomechanical motion and permanently relief of the lower back pain of the human [91-93]. There are two types total disc replacement implants: non-tissue engineered and tissue engineered. Non-tissue engineered total disc replacement implants (only two FDA approved implants: SB Charite and ProDisc[94]) use a combination of metal and polymers. These disc often lead to mechanical failure, dislodgement, wear associated osteolysis and implant

loosening[95]. Due to the recent progress in cell biology to determine the nature of the NP, AF and cartilage cells at EP, increasing attention has been turned toward creating tissue-engineered total disc replacement implants[95]. The ability of AF cells to remodel and grow in fibrous matrices as well as the ability of NP cells to assemble hydrogel based extracellular matrix lead to the fabrication of tissue-engineered IVD implants to regenerate AF and NP tissue as a unit[96]. Despite the promise of tissue engineering approaches for design of tissue-engineered IVD, there is only one FDA approved IVD in the market (Raymedica prosthetic disc nucleus (PDN))[97]. The reason for this limited number of commercial tissue-engineered total disc replacement implant is that this implant are unable to withstand the long-term physiological load [94]. Currently researched tissue-engineered IVD are composed of an outer shell of fiber mesh seeded with AF cells with an inner core of NP cells seeded into hydrogen [95, 96, 98-100]. Since EP carries significant deformations even under relatively low-loading conditions [101-103], therefore, tissue-engineered IVD construct must include the EP scaffold in addition to NP and AF scaffold. No study has been conducted to evaluate whether the addition of EP scaffold to the tissue-engineered IVD influence the biomechanical functions of the IVD. Such inclusion of EP layer in the tissue engineered IVD may solve the inability of the IVD to withstand the long-term physiological load. The proposed project will create a novel composite tissue-engineered IVD implant where AF and EP scaffolds will be coupled with a NP gel. Also the project will evaluate if the designed IVD satisfy the long-term biomechanical functions as like as a natural disc.

7.3 Material and Method

7.3.1 Introduction

This study shows a novel electrospun process to produce electrospun fiber-anchored NP gels and shows the design of a novel engineered IVDs. This invention shows a unique tissue-engineered IVD that can be used for the fabrication of both non-tissue and tissue engineered IVDs. This invention shows a 4 steps process by which both non- tissue engineered and tissue engineered IVD can be fabricated for degenerated IVD

diseases. The uniqueness of the invention is the use of PCL electrospun PCL nanofiber mesh to anchor the NP. In addition, this invention can create angle ply AF structure around the circumference of NP to mimic the architecture of native IVD. Finally, the invention anchored the top and bottom sides of NP by random fiber mesh that can used to create scaffold for the generation of endplate tissue.

7.3.2 Fabrication steps

7.3.2.1 Production of nucleus pulposus (NP) disc

(a)NP disc Material type 1: Silicone

Materials

The materials used for the silicone synthesis include responsive silicone gel system base, (implant grade), and the responsive silicone gel system crosslinker (implant grade). The silicone gel system was selected to model the nucleus pulposus of the intervertebral disc. Silicone gel was prepared by mixing a 40 wt% of poly-dimethyl-hydogen-siloxane crosslinker agent with polydimethylvinylsiloxane base. Both base and crosslinker were purchased from Applied Silicone Corporation.

Instrumentation

The instrumentation used for the silicone synthesis includes a 100 mL beaker, VWR vacuum oven, VWR single channel pipette (variable volume), and aluminum curing mold, glass stirring rod, and an analytical balance.

Method

The silicone synthesis process is shown in Figure 6 below. The silicone was prepared using a 73.2% to 26.8% by weight ratio of silicone system base and silicone system crosslinker, respectively. The silicone base and silicone crosslinker were weighed and measured with the scale and VWR pipette, then mixed in 100 mL beaker for 20 minutes where the solution was stirred manually with a glass stirring rod. The solution was then placed in the VWR vacuum oven for 10 minutes at 20 cm Hg vacuum to remove the air bubbles from the solution. Once the air bubbles were removed, the silicone solution was removed from the oven and into the aluminum molds with the use of the VWR pipette. The aluminum mold was then placed in the VWR vacuum oven at 160°C and 20 cm Hg for 3 hours for curing. The silicone mold was allowed to cool and removed from the oven at which the silicone disc model was removed from the mold and prepared for nano-fiber application. The process is shown in Figure 7-2. The inventors have successfully fabricated 10 mm diameter and 5 mm thickness silicone gel using the process.

(b)NP disc Material type 2: PEGDA

Materials

Two solution, PEGDA (M_n =700; Sigma-Aldrich) with the Phosphate Buffer Solution (PBS) solvents, and the photo initiator (PI), Alpha-alpha-dimethoxy-alpha-phenylacetophenone (M_w =256.35 g/mol; Sigma-Aldrich) with the 1-vinyl-2-pyrrolidone (M_w =111.14 g/mol; Fluka) solvents, were used to fabricate the gel solutions. PBS was used instead of water in this study, since PBS is better biological solvent than water when preparing cell encapsulating PEGDA gel.

Methods

Figure 7-3 shows the steps used for the preparation of the mold and specimen. 20% PEGDA in PBS mixture was added to the 0.2% concentration of photoinitiator mixture to prepare the PEGDA solution. The PEGDA solution was poured in a custom made plastic syringe chamber, where there is through hole at the center of the plunger. The hole is used to support a conductive wire. A silicone pad(Casting Craft Easymold Silicone

Rubber, Environmental Technology Inc. Fields Landing, CA) was glued on the top of the pushing rod. The silicone disc prevents leakage of PEGDA solution from the syringe chamber. A conductive wire was inserted through the plunger hole up to the top of the syringe chamber.The solution was poured in the syringe chamber to cure the mixture in a round shape gel. The photo-polymerization system used in the invention is comprised of three major parts: 1) a UV light source, 2) plastic syringe mold and 3) a polymer solution inside the syringe chamber (Figure 7-4 (a). The role of the mold is to allow the PEGDA to polymerize in the desired shape. The solution was polymerized by exposure to 365nm long wave UV (B-100SP Ultraviolet Lamp, UVP, LLC) light for 3 minutes. The plunger was pushed out to free the PEGDA disc from the syringe chamber. The inventors have successfully fabricated 10 mm diameter and 3 mm thickness PEGDA disc (Figure 7-4 (b)).

(c)NP disc Material type 3: PCL/PEGDA composite disc

Three layers of PEGDA-PCL composite scaffold were fabricated using a manually operated electrospun setup and UV photo-polymerization unit as discussed in detail in chapter 6.

7.3.2.2 Coating on top and circumferential surface of the NP disc by random fiber

All the above different kinds of NP disc were coated with random fiber at the top and circumferential sides by mutli-layers of random fiber in the custom made plastic syringe. Figure 7-5 shows the coating of all NP disc in top and circumferential sides by random PCL fibers. The embodiment shown in the diagram includes the sealed chamber, a syringe pump, a syringe with a tube that is attached with a non-conducting support, a syringe needle at the end of the tube, a high voltage power supply, and custom made plastic syringe containing the NP disc. The syringe needle is electrically charged by applying a high-voltage in the range of (5 KVA to 15 KVA) produced by the power supply. An opposed charge is applied to the conductive wire at the center of the custom made syringe by applying a high-voltage in the range of generated by the power supply.

(a)Coating on the bottom surface of the NP disc by random fiber

The NP disc is placed again in the plastic chamber with the conductive wire inserted at the center. The bottom side of NP that didn't have PCL fiber mesh is faced up so that the random fiber can be coated on that side. Multiple layers of random fibers are deposited on the side. Figure 7-6 shows the coating of NP disc by random fibers in the side where there is no existence of fiber coating. Figure 7-7 shows the resultant product where NP disc was every side by multilayers of random fiber.

(b) Coating on circumferential surface of the disc by aligned fiber

The process concludes with the disc being completely encased with an electrospun nanofiber membrane to support the various kinds of NP disc. The disc is wrapped with a 60 degree angle ply band constructed of electrospin microfibers to mimic natural IVD annual fibrosus (AF) (Figure 7-8). The AF that comprises discrete fibrous sheets with specialized collagen alignment bears the multi-directional loads around the circumference. Fibers run in a single direction in native AF tissue, ranging from 20º to 60º with respect to the transverse plane, and adjacent lamellae have opposing fiber orientations, producing an angle-ply structure

There are two ways the angle ply fibrous structures as depicted in Figure 7-8 can be produced along the circumference of the NP disc. One method is to by rotate the plastic syringe plunger that contains the disc at + and - 60 degree angles with respect to the aligned fiber collected between two wires to create the angle ply structures (Figure 7-9 (a)). The other method is to collect the aligned fiber between two wires in a stand. The aligned fiber membrane can be oriented + and - 60 degree angles to coat the NP disc using the angle ply fibrous structures (Figure 7-9 (b)). The NP disc can be mounted vertically for the second case.

This invention used first method to create multilayers of angle ply structures around the circumference of NP disc. Aligned PCL angle ply structure were deposited on the NP disc by manually rotating the NP disc 6 times (+ and – 60 degrees) and dried in UV

chamber. After application of 6 layers of angle ply structure on the NP disc, the disc was soaked with collagen solution. Collagen solution was prepared by mixing 2.3 microliter of type I collagen with 0.23 microliter of acetic acid (2%) and 195 microliter of deionized water in a vortex mixer. The above application of CG and PCL coating on NP were repeated 3 times to get our engineered IVD.

7.3.2.3 Production of Engineered IVD

(a)Silicone IVD (non-tissue engineered IVD)

No further processing is required for silicone IVD for the implantation in the spine where PCL electrospun nanofiber anchored silicone NP material in all sides.

(b)PEGDA based tissue engineered IVD

Polyethylene Glycol Diacrylate (PEGDA) tissue scaffolds having thickness higher than 1 mm were shown to have limited applications as a three-dimensional cell culture device due to the inability of cells to survive within the scaffolds [90]. Without access to adequate nutrients, cells placed deep within the PEGDA tissue construct having thickness higher than 1 mm die out, leading to nonuniform tissue regeneration. Since PEGDA material has high degradation rate in compare to PCL fiber materials, therefore, the PEGDA IVD can be soaked with PBS or HBSS solution for couple of weeks at 38 degree centigrade in an incubator (Figure 7-10). When PEGDA material fully disintegrated, any NP cell seeded hydrogel material can be injected to the IVD maintaining the standard cell culture conditions. After appropriate period of cell culture, the IVD will be ready for the implantation in the spine.

In this invention, the degradation of PEGDA was observed within couple of days after soaking our invented PEGDA IVD in PBS in an incubator (Figure 7-11). We have successfully injected silicone after the PEGDA disintegrated inside the PCL enclosure.

(c)PCL/PEGDA composite tissue engineered IVD

Applying appropriate cell culture protocols, NP, AF and cartilage cells can be seeded in to PCL/PEGDA composite NP scaffold, the angle ply structure and end plates. After appropriate time of cell culture, the PCL/PEGDA composite engineered IVD can be implanted in the spine.

7.3.3 Mechanical tests on silicone EIVD

7.3.3.1 Sample preparation

The PCL acetone polymer solution used in the fiber production. The solution was prepared using a 92.3% to 7.7% by weight ratio of acetone and PCL, respectively. The dimension of gel and fiber layers in the EIVD is equipment to the NP and AF dimension of a rabbit tail at caudal disc 4 (found from CT image of a rabbit tail Figure 7-12 (a)).

7.3.3.2 Compressive and Rheological tests

Evex compression test setup was used to find the gel compressive modulus. The gel was compressed to 80% of the gel height at a rate 0.05 mm/sec during the unconfined compression tests. Viscosity and oscillation tests were performed on the hydrogel using the Malvern CVO-100 rheometer at 5%, 10%, and 15% strain rate at frequency 1 Hz. Viscous, elastic and complex modulus was found from the experiment.

7.3.4 *Ex vivo* mechanical tests of silicone EIVD using rabbit caudal spine

7.3.4.1 Sample preparation

Two caudal (Cd) vertebral (Cd1-Cd7) spines were collected from female New Zealand White Rabbits. All rabbits were euthanased when approximately 3 months of old (weight range, 3.2–3.8 kg) as part of Dr. Khandaker ongoing grant support from OK-INBRE (Oklahoma IDeA Network of Biomedical Research Excellence). The experiment has been approved by the Institutional Animal Care and Use Committee (IACUC) - University of Oklahoma Health Sciences Center. Each rabbit had a titanium implant on femur for 8 weeks and there was no known history of back pathology. CT scan images (Figure 7-12 (a)) of spinal specimens (Figure 7-12 (a)) were used to identify the location

of discectomy and EIVD insertion site at caudal vertebral column. Immediately after euthanasia, the spinal specimens were harvested and frozen at -20ºC. Prior to testing, each frozen specimen was thawed at 4ºC (24 h) and cleared of all soft tissue. The specimens were divided into two groups, with group 1 containing a native spinal specimen and group 2 containing spinal specimen after discectomy and insertion of the EIVD at Cd 4 (Figure 7-12 (b)). The annular incision was closed using suture (Figure 7-12(c)).

7.3.4.2 Mechanical testing

The Cd 2 vertebras were embedded in a metal cup by BioMedtrix 3 veterinary bone cement. After 30 minutes of curing of the cement, the embedded spinal specimens were fastened at the top gripper in Test Resources UTM. Another same size metal cup was secured in the bottom gripper and bone cement was poured in to the cup. The top metal cup with the embedded spine were lowered till the Cd5 is completed covered by the bottom cup cement. Due to the low viscosity of the bone cement, negligible pre-load was applied to spine during the anchoring of the spine to the bottom cup (Figure 7-12 (d)). After 30 minutes of curing, each sample was compressed by 5 sequential 3% of strain increments from 3% to 15% strain. After each increment, the load and displacement data was recorded.

7.4 Results

7.4.1 Mechanical tests on silicone EIVD

Table 7-1 shows that the compressive modulus, complex shear modulus and phase shift angle of silicone gels and EIVD, which are in the range of human NP. These results confirm the suitability of electrospun fiber anchorage to gels, since it improves the mechanical properties of the gels. In addition, a wide range of viscoelastic silicone gels can be produced by varying the amount of cross-linker agents with base.

7.4.2 Ex vivo mechanical tests of silicone EIVD using rabbit caudal spine

The results (Figure 7-12(e)) show EIVD can able to restore the compressive load behavior of native rat caudal spine. These results are in consistence with the in vitro results. Dynamic mechanical behavior of the motion segments after in vivo implantation of EIVD will provide further proof the restoration capability of the EIVD.

7.5 Conclusions

This study successfully produced a novel EIVD using electrospun fiber mimicking the size of NP and AF at rabbit tail spine. Any size of EIVD can be produced using the unique electrospin technique (filled for a provisional patent). Angle ply fiber cloth mimicking the AF architecture is also produced. The results suggested that silicone EIVD are suitable as the replacement disc and should be studied further for the feasibility in IVD application.

7.6 Figures

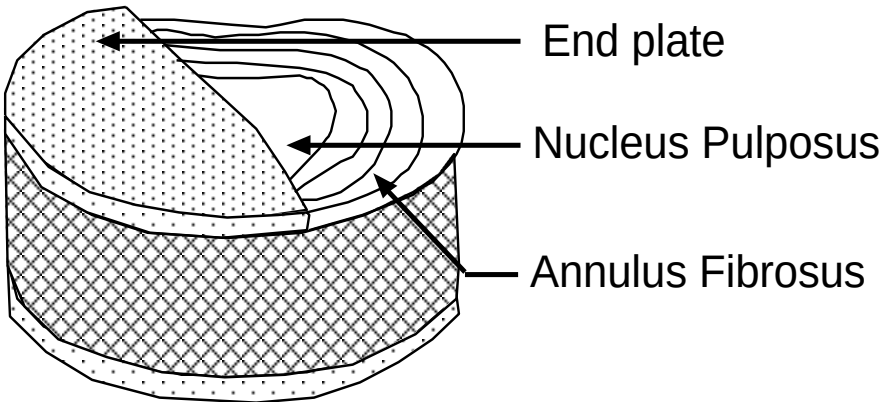

Figure 7-1 Schematic representation of different components of IVD

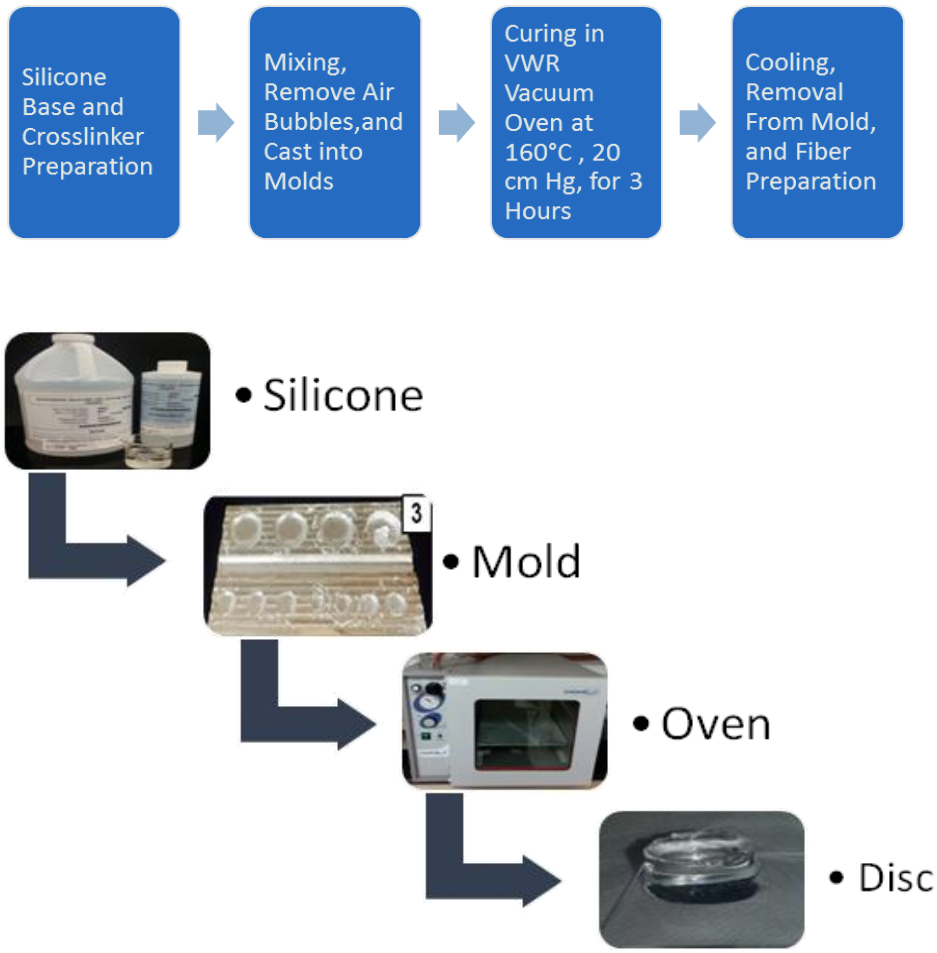

Figure 7-2: Silicone Synthesis and Disc Procedure

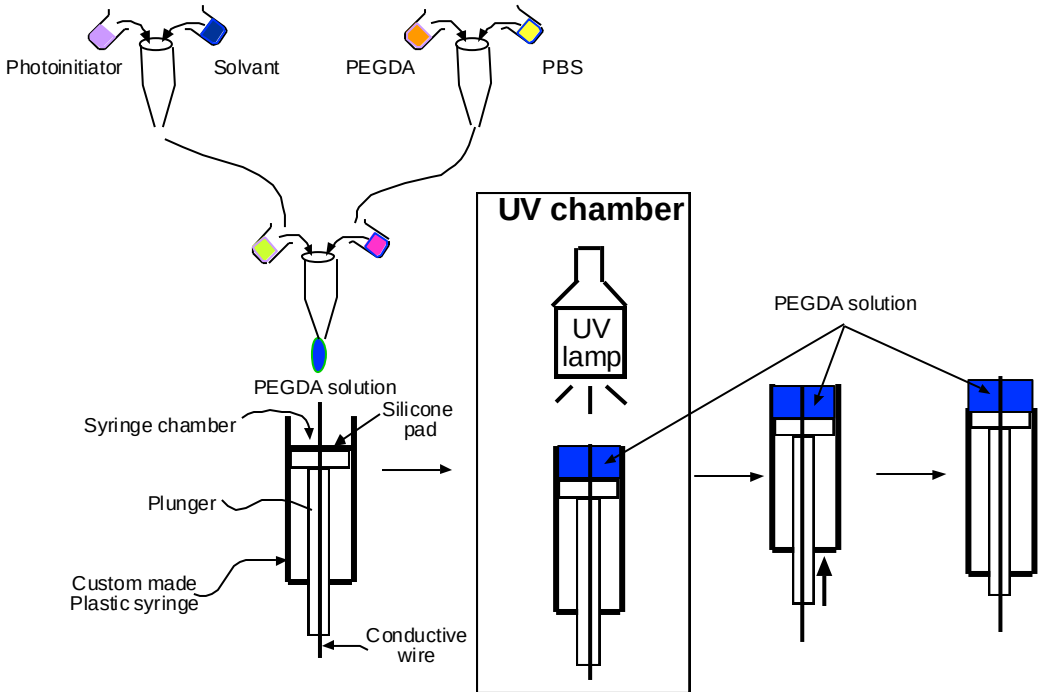

Figure 7-3 PEGDA Synthesis and Disc Procedure

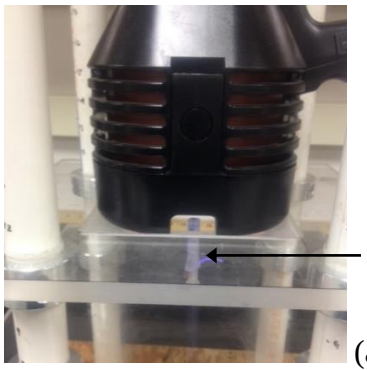

(a)

(b)

Figure 7-4 (a) Curing of PEGDA solution in a custom made plastic syringe at the UV chamber and (b) produced PEGDA disc that was pushed out from the plastic syringe chamber

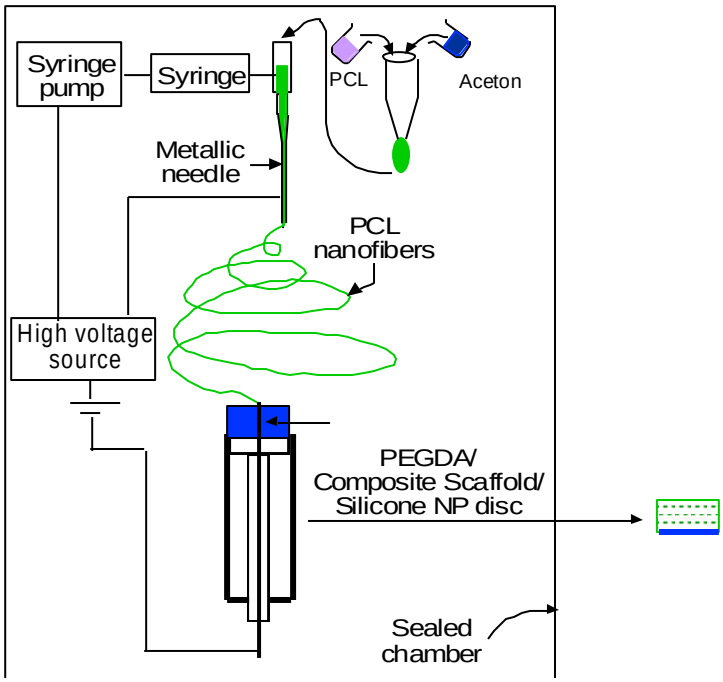

Figure 7-5 Coating of NP disc in top and circumferential sides by random fibers

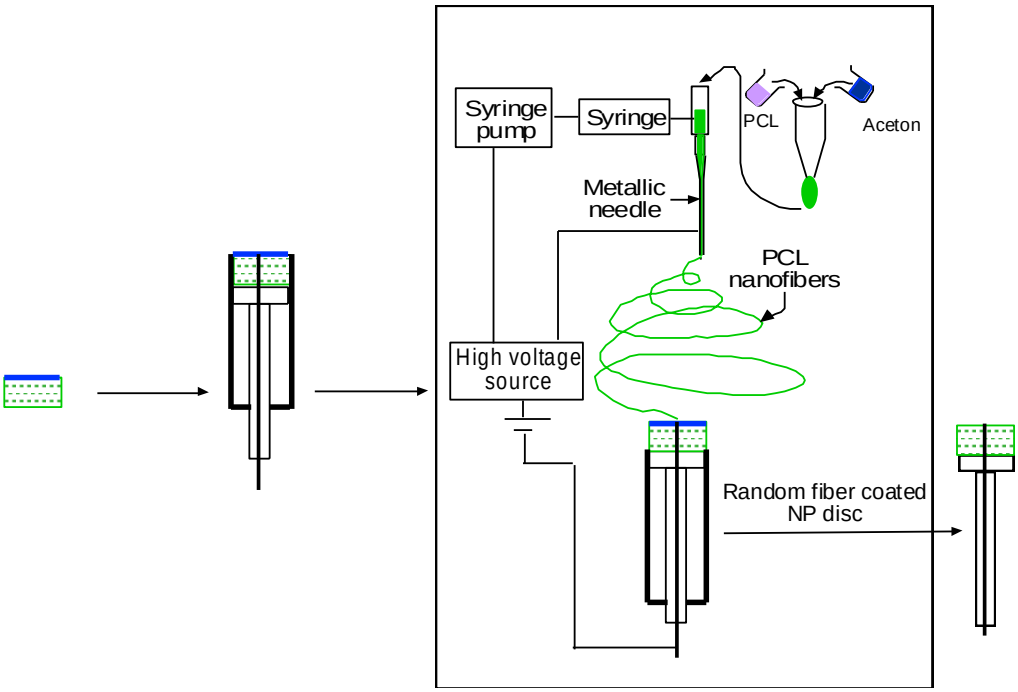

Figure 7-6 Coating of NP disc by random fibers in the side where there is no existence of fiber coating

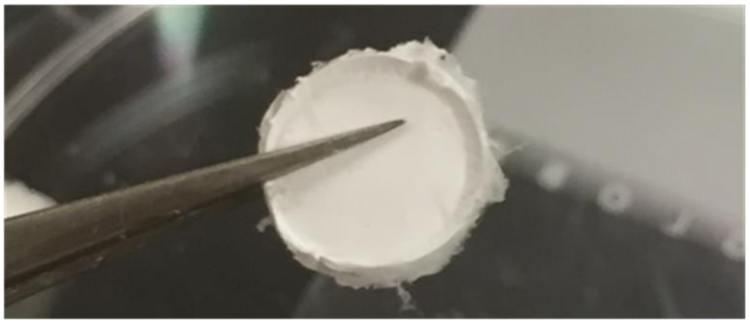

Figure 7-7 Coating of NP disc by random fibers

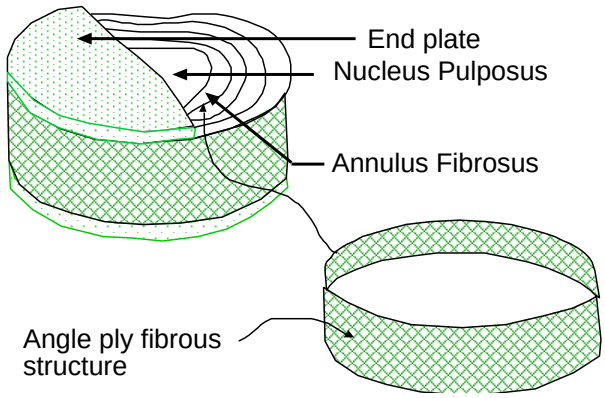

Figure 7-8 Components of the engineered IVD that mimic the architecture of natural IVD.

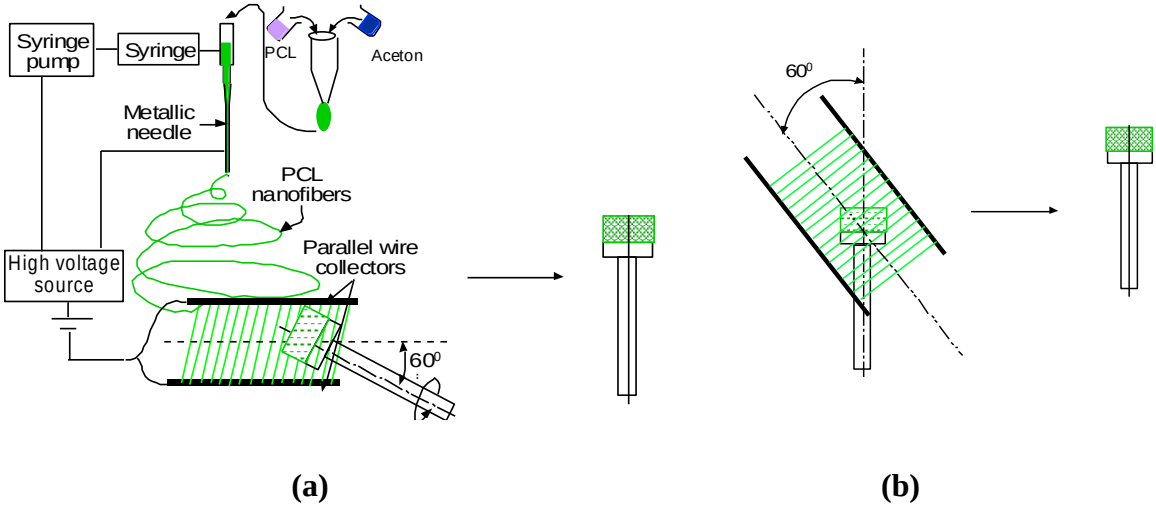

Figure 7-9 Production of angle ply structure on the circumference of NP disc.

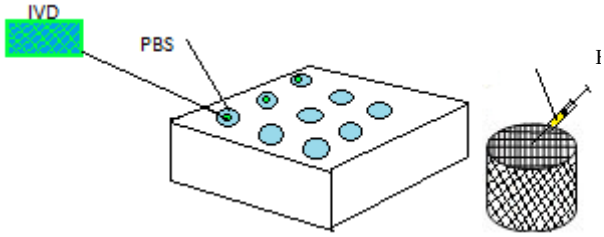

Figure 7-10 Preparation of PEGDA based tissue engineered IVD

Figure 7-11 PEGDA IVD in PBS solution at 38 degree centigrade in an incubator.

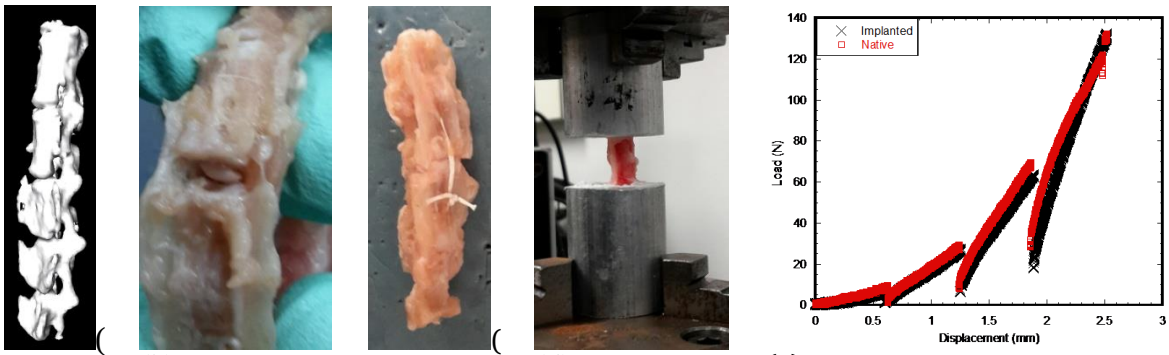

a) (b) c) (d) (e)

Figure 7-12 (a) CT scan image of a rabbit tail, (b) IVD implantation on rabbit tail, (c) sutured tail having IVD implant, (d) sample in a Test Resource UTM, and (e) load-displacement curve of native and implanted samples.

7.7 Tables

Table 7-1 Difference between viscoelastic properties between silicone gel and human NP materials.

Experimental parameters	Human NP	Silicone gel	Silicone IVD
Compressive modulus (kPa)	64.9 ± 44.1[104]	38.75	87.47
Complex modulus (kPa)	7 ~ 20[105]	0.133± 0.006	26.54 ± 7.54
Phase shift angle (degree)	23~ 30[105]	27.52± 0.83	21.73± 7.99

CHAPTER 7

CONCLUSION AND FUTURE WORKS

8.1 Conclusions

The goal of this research is to improve the mechanical and biological functions of metallic and polymeric implants by Nanotopographical modifications of implant surface. This study used three nanotopographical modifications techniques; Laser peening, plasma nitridation and electrospun nanofiber coating techniques were used to improve the mechanical and biological functions of titanium implant.

This study concluded that the laser peen treatment significantly changed the nano architecture of Ti samples, which lead to mechanical stability of Ti with PMMA bone cement.

This research shows that the nitrogen plasma treatment influenced the hardness, and energy of conventional Ti-cement interfaces, which lead to the enhancement of the bonding of Ti alloy with bone cement compared to the untreated samples. DC glow discharge plasma nitriding treatment on Ti surface can potentially improve the union between Ti-cement interfaces.

This study established a proof of concept of microgrooving on Ti and CG-PCL coating of the grooves for improving the mechanical stability and osseointegration of an orthopedic implant. Also, this study shows that the combined application of microgroove and extracellular matrix structure enhanced the mechanical interlock and osseointegration of an implant with the host tissue. The fabrication of surface microgrooves on Ti and local delivery of extracellular matrix protein (collagen) at the microgrooves sites allowed the increase of the mechanical interlock and biocompatibility of a Ti implant. Moreover, the present study showed that the increase in peri-implant new bone volume is increased due to NFM coating. Therefore, implant

surface modification by groove-associated bio coating can potentially improve orthopedic implants mechanical and biological responses with surrounding biomaterials.

This research concluded that MgO nanoparticle has positive influence on the mechanical stability of the Ti/PMMA interfaces. Therefore, MgO nanoparticle has potential to be used with PMMA cement for cemented implant surgeries.

The test results showed that the higher surface artifacts of PCL-PEGDA composite scaffold in compare to PEGDA scaffold. The stiffness of PCL-PEGDA composite scaffold is approximately 2 times higher in compare to PEGDA scaffold. The results indicts that PCL-PEGDA composite scaffold strength should be higher compare to of this study confirms that PCL ENF membrane reinforced the PEGDA scaffold. We have successfully fabricated 10 mm diameter and 1.5 mm thickness composite hydrogel. The invented composite scaffold fulfills good mechanical strength and superior microstructure requirements for tissue substitutes.

This study successfully produced a novel EIVD using electrospun fiber mimicking the size of NP and AF at rabbit tail spin. Any size of EIVD can be produced using the unique electrospin technique. Angle ply fiber cloth mimicking the AF architecture is also produced. The results suggested that silicone EIVD are suitable as the replacement disc and should be studied further for the feasibility in IVD application.

8.2 Future works

The future works for chapter 2 is to change the specification of laser peening and developed alternative of nano architecture of Ti samples such as size, distance, depth, arrange of spots.

Future work for chapter 3 is to see the effect of nanoparticle such as MgO on this result.

In future study for chapter 4, groove with PCL-CG will be further investigated with consistent and biocompatible groove that will be created by micron ridges using nanofabrication technology.

Future work for chapter 5 is to in vivo evaluation of the other nanoparticles effect on titanium/cement interfaces. Nanoparticle such as CT, HA, Chitoson, $Baso_4$, Sio_2, Can add to into the PMMA to modify the bone cement.

The future work for chapter 6 is in vivo evaluation of a composite hydrogel scaffold as a bone graft.

Future work for chapter 7 is in vivo evaluation of electrospin fiber anchored intervertebral disc implant

REFERENCES

[1] Z.-M. Huang, Y. Z. Zhang, M. Kotaki, and S. Ramakrishna, "A review on polymer nanofibers by electrospinning and their applications in nanocomposites," *Composites Science and Technology,* vol. 63, pp. 2223-2253, 11// 2003.

[2] J. M. Deitzel, J. Kleinmeyer, D. Harris, and N. C. Beck Tan, "The effect of processing variables on the morphology of electrospun nanofibers and textiles," *Polymer,* vol. 42, pp. 261-272, 1// 2001.

[3] A. K. Haghi, *Electrospun Nanofibers Research*. Hauppauge, US: Nova Science Publishers, Inc., 2009.

[4] T. Fett, "Stress intensity factors for edge-cracked plates under arbitrary loading," *Fatigue & Fracture of Engineering Materials & Structures,* vol. 22, pp. 301-305, Apr 1999.

[5] D. M. Brunette, P. Tengvall, M. Textor, and P. Thomsen, *Titanium in Medicine: Material Science, Surface Science, Engineering, Biological Responses and Medical Applications*, 1 ed., 2001.

[6] A. B. Lennon, B. A. O. McCormack, and P. J. Prendergast, "The relationship between cement fatigue damage and implant surface finish in proximal femoral prostheses," *Medical Engineering and Physics,* vol. 25, pp. 833-841, 2003.

[7] L. J. Elias CN, Valiev R, Meyers MA, "Biomedical applications of titanium and its alloys," *JOM,* vol. 60, pp. 46-49, 2008.

[8] H. H. O. Okuno, *Dent. Jpn.,* vol. 26, pp. 101-104, 1989.

[9] G. Cunin, H. Boissonnet, H. Petite, C. Blanchat, and G. Guillemin, "Experimental vertebroplasty using osteoconductive granular material," *Spine (Phila Pa 1976),* vol. 25, pp. 1070-6, May 1 2000.

[10] Z. W. H. J.X. Lu, P. Tropiano., "Human biological reactions at the interface between bone tissue and polymethylmethacrylate cement," *J Mater Sci Mater Med,* vol. 13, pp. 803-809, 2002.

[11] J. E. Barralet, K. J. Lilley, L. M. Grover, D. F. Farrar, C. Ansell, and U. Gbureck, "Cements from nanocrystalline hydroxyapatite," *Journal of Materials Science: Materials in Medicine,* vol. 15, pp. 407-411, 2004.

[12] F. Javier Gil, J. A. Planell, A. Padros, and C. Aparicio, "The effect of shot blasting and heat treatment on the fatigue behavior of titanium for dental implant applications," *Dent Mater,* vol. 23, pp. 486-91, Apr 2007.

[13] R. Fathallah, A. Laamouri, H. Sidhom, and C. Braham, "High cycle fatigue behavior prediction of shot-peened parts," *International Journal of Fatigue,* vol. 26, pp. 1053-1067, 10// 2004.

[14] A. Anders, "Metal plasma immersion ion implantation and deposition: a review," *Surf. Coat. Technol.,* vol. 93, pp. 158–167, 1997.

[15] J. A. Bishop, A. A. Palanca, M. J. Bellino, and D. W. Lowenberg, "Assessment of compromised fracture healing," *J Am Acad Orthop Surg,* vol. 20, pp. 273-282, 2012.

[16] "idataresearch.com, U.S. Orthopedic Trauma Devices Market," 2013.

[17] J. R. T. Jeffers, M. Browne, A. B. Lennon, P. J. Prendergast, and M. Taylor, "Cement mantle fatigue failure in total hip replacement: Experimental and computational testing," *Journal of Biomechanics*, vol. 40, pp. 1525-1533, 2007.

[18] S. W. Gravius, D.C. ; Siebert, C.H. ; Andereya, St. ; Mueller-Rath, R. ; Maus, U. ; Mumme, T., "In vitro interface and cement mantle analysis of different femur stem designs " *Journal of Biomechanics*, vol. 41, pp. 2021-2028, 2008.

[19] A. S. Ramos, J.A., "The influence of cement mantle thickness and stem geometry on fatigue damage in two different cemented hip femoral prostheses," *Journal of Biomechanics*, vol. 42, pp. 2602-2610, 2009.

[20] F. Al Mansour, N. Karpukhina, S. Grasso, R. M. Wilson, M. J. Reece, and M. J. Cattell, "The effect of spark plasma sintering on lithium disilicate glass-ceramics," *Dental Materials*.

[21] S. L. Christensen, J. D. Padmos, A. Chatt, and P. Zhang, "Preparation and Orthopaedic Applications of Nanoparticle-Modified Biocompatible Surfaces," *Reviews in Nanoscience and Nanotechnology*, vol. 2, pp. 63-78, // 2013.

[22] K. L. Ohashi, A. C. Romero, P. D. McGowan, and M. T. Maloney, "Adhesion and reliablity of interfaces in cemented total joint arthroplasties," *Journal of orthopedic research*, vol. 16, pp. 705-714, 1998.

[23] Y. K. K. Hosein, Graham J. W. ; Dunning, Cynthia E., "The Effect of Stem Circumferential Grooves on the Stability at the Implant-Cement Interface," *Journal of Medical Devices*, vol. 8, p. 014504, 2014.

[24] M. T. Manley, L. S. Stern, and J. Gurtowski, "The load carrying and fatigue properties of the stem-cement interface with smooth and porous coated femoral components," *J Biomed Mater Res*, vol. 19, pp. 563-75, May-Jun 1985.

[25] A. H. Fritsche, Maximilian ; Zietz, Carmen ; Mittelmeier, Wolfram ; Neumann, Hans-Georg ; Heidenau, Frank ; Finke, Birgit ; Bader, Rainer, "Mechanical characterization of anti-infectious, anti-allergic, and bioactive coatings on orthopedic implant surfaces," *Journal of Materials Science*, vol. 44, pp. 5544-5551, 2009.

[26] A. Laamouri and R. Fathallah "High Cycle Fatigue Behavior Prediction Of Shot Peened Parts " *International Journals of Fatigue* vol. 26, pp. 1053 - 1067, 2004.

[27] R. Kasinath, A. Braizer, K. H. Prakash, and L. Gower, "Hierarchical assembly of hybrid nanoapatites: Implications for oral drug delivery and implant-biological interfaces," in *Processing of Nanoparticle Structures and Composites - 2008 Materials Science and Technology conference, MS and T08, October 5, 2008 - October 9, 2008*, Pittsburgh, PA, United states, 2009, pp. 123-132.

[28] I. LSP Technologies. (2013). *How Laser Peening Works*. Available: http://www.lsptechnologies.com/how-laser-peening-works.php

[29] Moffat KL, Wang IN, Rodeo SA, and L. HH., "Orthopedic interface tissue engineering for the biological fixation of soft tissue grafts," *Clin Sports Med.*, vol. 28, pp. 157-76, 2009

[30] H. Lu, S. Subramony, M. Boushell, and X. Zhang, "Tissue Engineering Strategies for the Regeneration of Orthopedic Interfaces," *Annals of Biomedical Engineering*, vol. 38, pp. 2142-2154, 2010.

[31] M. Nikkhah, F. Edalat, S. Manoucheri, and A. Khademhosseini, "Engineering microscale topographies to control the cell–substrate interface," *Biomaterials,* vol. 33, pp. 5230-5246, 2012.
[32] M. Biggs, M. Dalby, C. Wilkinson, N. Gadegaard, and G. Richards, "The influence of nanoscale structures on osteoblast adhesion," *Comparative Biochemistry and Physiology - Part A: Molecular & Integrative Physiology,* vol. 146, p. S191, 2007.
[33] L. Prodanov, J. te Riet, E. Lamers, M. Domanski, R. Luttge, J. J. W. A. van Loon, *et al.*, "The interaction between nanoscale surface features and mechanical loading and its effect on osteoblast-like cells behavior," *Biomaterials,* vol. 31, pp. 7758-7765, 2010.
[34] A. Kapoor, E. H. G. Caporali, P. J. A. Kenis, and M. C. Stewart, "Microtopographically patterned surfaces promote the alignment of tenocytes and extracellular collagen," *Acta Biomaterialia,* vol. 6, pp. 2580-2589, 2010.
[35] V. Mathieu, R. Vayron, G. Richard, G. Lambert, S. Nail, J.-P. Meningaud, *et al.*, "Biomechanical determinants of the stability of dental implants: Influence of the bone-implant interface properties," *Journal of Biomechanics,* vol. 47, pp. 3-13, 2014.
[36] J. Davies and W. Harris, "Strength of cement-metal interfaces in fatigue: comparison of smooth, porous and precoated specimens," *Clinical Materials,* vol. 12, pp. 121-6, 1993.
[37] T. Lu, Y. Qiao, and X. Liu, "Surface modification of biomaterials using plasma immersion ion implantation and deposition," *Interface Focus,* vol. 2, pp. 325-36, Jun 6 2012.
[38] Y. Adriaensen, C. Dupont-Gillain, S. Derclaye, and P. Rouxhet, "Plasma-oxidized polystyrene: wetting properties and surface reconstruction," *Langmuir,* vol. 16, pp. 8194-200, 2000.
[39] J. X. Lu, Z. W. Huang, P. Tropiano, B. Clouet D'Orval, M. Remusat, J. Dejou, *et al.*, "Human biological reactions at the interface between bone tissue and polymethylmethacrylate cement," *J Mater Sci Mater Med,* vol. 13, pp. 803-9, Aug 2002.
[40] H. M. Wong, Y. Zhao, V. Tam, S. Wu, P. K. Chu, Y. Zheng, *et al.*, "In vivo stimulation of bone formation by aluminum and oxygen plasma surface-modified magnesium implants," *Biomaterials,* vol. 34, pp. 9863-9876, 2013.
[41] K. Jonsson, J. Köhler, C. Hedlund, and L. Stenmark, "Oxygen plasma wafer bonding evaluated by the Weibull fracture probability method," *Journal of Micromechanics and Microengineering,* vol. 11, pp. 364-370, Jul 2001.
[42] W. R. Walsh, M. J. Svehla, J. Russell, M. Saito, T. Nakashima, R. M. Gillies, *et al.*, "Cemented fixation with PMMA or Bis-GMA resin hydroxyapatite cement: Effect of implant surface roughness," *Biomaterials,* vol. 25, pp. 4929-4934, 2004.
[43] Bhehler, "Application Guide Polishing: Solutions for Materials Preparation, testing and analysis," ed, 2012.
[44] M. Khandaker, S. Riahinezhad, F. Sultana, M. Vaughan, J. Knight, and T. Morris, "Peen treatment on a titanium implant: effect of roughness, osteoblast cell

functions, and bonding with bone cement.," *International Journal of Nanomedicine,* 2016

[45] W.-S. Kim, I.-H. Yun, J.-J. Lee, and H.-T. Jung, "Evaluation of mechanical interlock effect on adhesion strength of polymer-metal interface," *International JournalofAdhesion&Adhesives,* vol. 30, pp. 408-417, 2010.

[46] E. P. Ferraz, J. C. Sa, P. T. De Oliveira, C. Alves Jr, M. M. Beloti, and A. L. Rosa, "The effect of plasma-nitrided titanium surfaces on osteoblastic cell adhesion, proliferation, and differentiation," *Journal of Biomedical Materials Research - Part A,* vol. 102, pp. 991-998, 2014.

[47] B. S. Yilbas, A. Z. Sahin, A. Z. Al-Garni, S. A. M. Said, Z. Ahmed, B. J. Abdulaleem, *et al.*, "Plasma nitriding of Ti-6Al-4V alloy to improve some tribological properties," *Surface and Coatings Technology,* vol. 80, pp. 287-292, 1996.

[48] E. Ferraz, A. Sverzut, G. Freitas, J. Sá, C. Alves, M. Beloti, *et al.*, "Bone tissue response to plasma-nitrided titanium implant surfaces.," *J Appl Oral Sci. ,* vol. 23, pp. 9-13, 2015.

[49] M. Khandaker, Y. Li , and T. Morris, "MgO micro/nano particles for the improvement of cement–bone interface," *journal of biomechanics,* vol. 46, pp. 1035–1039, 2013.

[50] (01/01/2014). *National Institutes of Health. Hip Replacement*. Available: http://www.niams.nih.gov/Health_Info/Hip_Replacement/

[51] *American Academy of Implant Dentistry. Dental Implants Facts and Figures*. Available: http://www.aaid.com/about/Press_Room/Dental_Implants_FAQ.html

[52] R. A. Gittens, T. McLachlan, R. Olivares-Navarrete, Y. Cai, S. Berner, R. Tannenbaum, *et al.*, "The effects of combined micron-/submicron-scale surface roughness and nanoscale features on cell proliferation and differentiation," *Biomaterials,* vol. 32, pp. 3395-3403, 2011.

[53] A. Travan, E. Marsich, I. Donati, M.-P. Foulc, N. Moritz, H. T. Aro, *et al.*, "Polysaccharide-coated thermosets for orthopedic applications: From material characterization to in vivo tests," *Biomacromolecules,* vol. 13, pp. 1564-1572, 2012.

[54] S. J. Heo, S. A. Park, H. J. Shin, Y. J. Lee, T. R. Yoon, H. Y. Seo, *et al.*, "Evaluation of bonding stress for the newly suggested bone cement: comparison with currently used PMMA through animal studies," *Key Engineering Materials,* vol. 342-342, pp. 373-6, 2007.

[55] S. Zankovych, M. Diefenbeck, J. Bossert, T. Mückley, C. Schrader, J. Schmidt, *et al.*, "The effect of polyelectrolyte multilayer coated titanium alloy surfaces on implant anchorage in rats," *Acta Biomaterialia,* vol. 9, pp. 4926-4934, 1// 2013.

[56] S. Kurtz, K. Ong, E. Lau, F. Mowat, and M. Halpern, "Projections of Primary and Revision Hip and Knee Arthroplasty in the United States from 2005 to 2030," *The Journal of Bone & Joint Surgery,* vol. 89, pp. 780-785, 2007-04-01 00:00:00 2007.

[57] S. Lenhert, M.-B. Meier, U. Meyer, L. Chi, and H. P. Wiesmann, "Osteoblast alignment, elongation and migration on grooved polystyrene surfaces patterned by Langmuir–Blodgett lithography," *Biomaterials,* vol. 26, pp. 563-570, 2005.

[58] B. J. Im, S. W. Lee, N. Oh, M. H. Lee, J. H. Kang, R. Leesungbok, *et al.*, "Texture direction of combined microgrooves and submicroscale topographies of titanium substrata influence adhesion, proliferation, and differentiation in human primary cells," *Archives of Oral Biology,* 2012.

[59] E. Lamers, X. Frank Walboomers, M. Domanski, J. te Riet, F. C. M. J. M. van Delft, R. Luttge, *et al.*, "The influence of nanoscale grooved substrates on osteoblast behavior and extracellular matrix deposition," *Biomaterials,* vol. 31, pp. 3307-3316, 2010.

[60] X. F. Walboomers, W. Monaghan, A. S. G. Curtis, and J. A. Jansen, "Attachment of fibroblasts on smooth and microgrooved polystyrene," *Journal of Biomedical Materials Research,* vol. 46, pp. 212-220, 1999.

[61] A. Pizzo, K. Kokini, L. Vaughn, B. Waisner, and S. Voytik-Harbin, "Extracellular matrix (ECM) microstructural composition regulates local cell-ECM biomechanics and fundamental fibroblast behavior: a multidimensional perspective," *J Appl Physiol,* vol. 98, pp. 1909-21, 2005.

[62] H. B. Wang, M. E. Mullins, J. M. Cregg, A. Hurtado, M. Oudega, M. T. Trombley, *et al.*, "Creation of highly aligned electrospun poly-L-lactic acid fibers for nerve regeneration applications," *Journal of Neural Engineering,* vol. 6, 2009.

[63] I. Keun Kwon, S. Kidoaki, and T. Matsuda, "Electrospun nano- to microfiber fabrics made of biodegradable copolyesters: structural characteristics, mechanical properties and cell adhesion potential," *Biomaterials,* vol. 26, pp. 3929-3939, 6// 2005.

[64] M. KHANDAKER and W. P. SNOW, "Method and apparatus for controlled alignment and deposition of branched electrospun fiber," 2016.

[65] G. H. Kim, "Electrospun PCL nanofibers with anisotropic mechanical properties as a biomedical scaffold," *Biomed Mater,* vol. 3, p. 025010, Jun 2008.

[66] I. K. Kwon, S. Kidoaki, and T. Matsuda, "Electrospun nano- to microfiber fabrics made of biodegradable copolyesters: structural characteristics, mechanical properties and cell adhesion potential," *Biomaterials,* vol. 26, pp. 3929-39, Jun 2005.

[67] Lodish H, Berk A, and Z. SL, "Collagen: The Fibrous Proteins of the Matrix," in *Molecular Cell Biology,* W. H. Freeman, Ed., 4 ed New York, 2000.

[68] W. He, Z. Ma, T. Yong, W. E. Teo, and S. Ramakrishna, "Fabrication of collagen-coated biodegradable polymer nanofiber mesh and its potential for endothelial cells growth," *Biomaterials,* vol. 26, pp. 7606-7615, 12// 2005.

[69] B. W. Tillman, S. K. Yazdani, S. J. Lee, R. L. Geary, A. Atala, and J. J. Yoo, "The in vivo stability of electrospun polycaprolactone-collagen scaffolds in vascular reconstruction," *Biomaterials,* vol. 30, pp. 583-588, 2// 2009.

[70] D. Buser, R. K. Schenk, S. Steinemann, J. P. Fiorellini, C. H. Fox, and H. Stich, "Influence of surface characteristics on bone integration of titanium implants. A

histomorphometric study in miniature pigs," *J Biomed Mater Res,* vol. 25, pp. 889-902, Jul 1991.
[71] I. Kanungo, N. N. Fathima, J. R. Rao, and B. U. Nair, "Influence of PCL on the material properties of collagen based biocomposites and in vitro evaluation of drug release," *Mater Sci Eng C Mater Biol Appl,* vol. 33, pp. 4651-9, Dec 1 2013.
[72] Bhehler, "Application Guide Polishing: Solutions for Materials Preparation, testing and analysis," ed, 2012.
[73] M. Khandaker, K. C. Utsaha, and T. Morris, "Interfacial fracture toughness of titanium-cement interfaces: Effects of fibers and loading angles," *International Journal of Nanomedicine,* vol. 9, 2014.
[74] J. D. Currey, *Bones: Structure and Mechanics*: Princeton University Press, 2002.
[75] P. Lucksanasombool, W. A. J. Higgs, R. Higgs, and M. V. Swain, "Interfacial fracture toughness between bovine cortical bone and cements," *Biomaterials,* vol. 24, pp. 1159-1166, Mar 2003.
[76] B. A. O. McCormack and P. J. Prendergast, "Microdamage accumulation in the cement layer of hip replacements under flexural loading," *Journal of Biomechanics,* vol. 32, pp. 467-475, 1999.
[77] A. Race, K. A. Mann, and A. A. Edidin, "Mechanics of bone/PMMA composite structures: An in vitro study of human vertebrae," *Journal of Biomechanics,* vol. 40, pp. 1002-1010, 2007.
[78] A. Race, M. A. Miller, D. C. Ayers, and K. A. Mann, "Early cement damage around a femoral stem is concentrated at the cement/bone interface," *Journal of Biomechanics,* vol. 36, pp. 489-496, 2003.
[79] X. D. Wang and C. M. Agrawal, "A mixed mode fracture toughness test of bone-biomaterial interfaces," *Journal of Biomedical Materials Research,* vol. 53, pp. 664-672, Dec 5 2000.
[80] J. D. Wood, P. I. Inigo, D. P. Thompson, and D. H. Pashley, "Mechanical behavior of the dentin-enamel interface," in *9th Intl. Cong. Soc. Experimental Mech.*, Orlando, FL, 2000, pp. 989-992.
[81] K. A. Mann and L. A. Damron, "Predicting the failure response of cement-bone constructs using a non-linear fracture mechanics approach," *Journal of Biomechanical Engineering-Transactions of the Asme,* vol. 124, pp. 462-470, Aug 2002.
[82] X. D. Wang and C. M. Agrawal, "Interfacial fracture toughness of tissue-biomaterial systems," *Journal of Biomedical Materials Research,* vol. 38, pp. 1-10, Spr 1997.
[83] Z. Shi, K. G. Neoh, E. T. Kang, and W. Wang, "Antibacterial and mechanical properties of bone cement impregnated with chitosan nanoparticles," *Biomaterials,* vol. 27, pp. 2440-2449, 2006.
[84] H. Liu and T. J. Webster, "Nanomedicine for implants: A review of studies and necessary experimental tools," *Biomaterials,* vol. 28, pp. 354-369, 01/10/ 2007.
[85] A. Ricker, P. Liu-Snyder, and T. J. Webster, "The influence of nano MgO and BaSO4 particle size additives on properties of PMMA bone cement," *International Journal of Nanomedicine,* vol. 3, pp. 125-1, 2008.

[86] S. Sirinrath and J. W. Thomas, "Multiwalled carbon nanotubes enhance electrochemical properties of titanium to determine in situ bone formation," *Nanotechnology,* vol. 19, pp. 95101-95101, 07/23/ 2008.

[87] M. Khandaker, M. Vaughan, T. Morris, J. White, and Z. Meng, "Effect of additives particles on mechanical, thermal and cell functions properties of poly (methyl methacrylate) cement," *Int J Nanomedicine,* vol. In Press, 2014.

[88] S.-H. Lee and H. Shin, "Matrices and scaffolds for delivery of bioactive molecules in bone and cartilage tissue engineering," *Advanced Drug Delivery Reviews,* vol. 59, pp. 339-359, 2007.

[89] I. C. Bonzani, R. Adhikari, S. Houshyar, R. Mayadunne, P. Gunatillake, and M. M. Stevens, "Synthesis of two-component injectable polyurethanes for bone tissue engineering," *Biomaterials,* vol. 28, pp. 423-433, 2007.

[90] O. Yasar, B. Starly, and S.-F. Lan, "A Lindenmayer systems based approach for the design of nutrient delivery networks in tissue constructs," *Journal of Biofabrication,* vol. 1, 2009.

[91] A. Van Ooij, F. C. Oner, and A. J. Verbout, "Complications of artificial disc replacement: a report of 27 patients with the SB Charité disc," *J Spinal Disord Tech,* vol. 16, pp. 369-83, 2003

[92] P. Kambin and M. H. Savitz, "Arthroscopic Microdiscectomy: An Alternative to Open Disc Surgery," *The Mount Sinai Journal of Medicine,* vol. 67, pp. 283-7, 2000.

[93] H. Weber, "Lumbar Disc Herniation: A Controlled Prospective Study with Ten Years of Observation," *Spine,* vol. 8, pp. 131-40, 1993.

[94] B. R. Whatley and X. Wen, "Intervertebral disc (IVD): Structure, degeneration, repair and regeneration," *Materials Science and Engineering: C,* vol. 32, pp. 61-77, 3/1/ 2012.

[95] M. Hirokazu, "Tissue-Engineered Composites of Anulus Fibrosus and Nucleus Pulposus for Intervertebral Disc Replacement," *Spine,* vol. 29, pp. 1290-1297, 2004.

[96] J. T. Martin, A. H. Milby, J. A. Chiaro, D. H. Kim, N. M. Hebela, L. J. Smith, *et al.*, "Translation of an engineered nanofibrous disc-like angle-ply structure for intervertebral disc replacement in a small animal model," *Acta Biomaterialia,* vol. 10, pp. 2473-2481, 6// 2014.

[97] A. J. Salgado, J. M. Oliveira, A. Martins, F. G. Teixeira, N. A. Silva, N. M. Neves, *et al.*, "Chapter One - Tissue Engineering and Regenerative Medicine: Past, Present, and Future," in *International Review of Neurobiology*. vol. Volume 108, I. P. P. T. Stefano Geuna and B. Bruno, Eds., ed: Academic Press, 2013, pp. 1-33.

[98] N. L. Nerurkar, S. Sen, A. H. Huang, D. M. Elliott, and R. L. Mauck, "Engineered Disc-Like Angle-Ply Structures for Intervertebral Disc Replacement," *Spine,* vol. 35, pp. 867-873, 2010.

[99] G. Vadala, P. Mozetic, A. Rainer, M. Centola, M. Loppini, M. Trombetta, *et al.*, "Bioactive electrospun scaffold for annulus fibrosus repair and regeneration," *Eur Spine J,* vol. 21 Suppl 1, pp. S20-6, May 2012.

[100] R. D. Bowles, H. H. Gebhard, R. Hartl, and L. J. Bonassar, "Tissue-engineered intervertebral discs produce new matrix, maintain disc height, and restore biomechanical function to the rodent spine," *Proc Natl Acad Sci U S A*, vol. 108, pp. 13106-11, Aug 9 2011.
[101] J. J. MacLean, J. P. Owen, and J. C. Iatridis, "Role of endplates in contributing to compression behaviors of motion segments and intervertebral discs," *Journal of Biomechanics*, vol. 40, pp. 55-63, 2007.
[102] R. L. Cynthia, "In Vitro Organ Culture of the Bovine Intervertebral Disc: Effects of Vertebral Endplate and Potential for Mechanobiology Studies," *Spine*, vol. 31, pp. 515-522, 2006.
[103] L. M. Boyd and A. J. Carter, "Injectable biomaterials and vertebral endplate treatment for repair and regeneration of the intervertebral disc," *European Spine Journal*, vol. 15, pp. 414-421, 2006.
[104] D. H. Cortes, N. T. Jacobs, J. F. DeLucca, and D. M. Elliott, "Elastic, permeability and swelling properties of human intervertebral disc tissues: A benchmark for tissue engineering," *J Biomech*, vol. 47, pp. 2088-94, Jun 27 2014.
[105] J. C. Iatridis, L. A. Setton, M. Weidenbaum, and V. C. Mow, "The viscoelastic behavior of the non-degenerate human lumbar nucleus pulposus in shear," *J Biomech*, vol. 30, pp. 1005-13, Oct 1997.